This document is the accepted manuscript version of the following article:

Bukowiecki, N., Weingartner, E., Gysel, M., Coen, M. C., Zieger, P., Herrmann, E., … Baltensperger, U. (2016). A review of more than 20 years of aerosol observation at the high altitude research station Jungfraujoch, Switzerland (3580 m asl). Aerosol and Air Quality Research, 16(3), 764-788. https://doi.org/10.4209/aaqr.2015.05.0305

A review of more than 20 years of aerosol observation at the high altitude research station Jungfraujoch, Switzerland (3580 m asl)

Nicolas Bukowiecki[1*], Ernest Weingartner[1‡], Martin Gysel[1], Martine Collaud Coen[2], Paul Zieger[1†], Erik Herrmann[1], Martin Steinbacher[4], Heinz W. Gäggeler[3], Urs Baltensperger[1]

[1] Laboratory of Atmospheric Chemistry, Paul Scherrer Institute, CH-5232 Villigen PSI, Switzerland

[2] Federal Office of Meteorology and Climatology, MeteoSwiss, Chemin de l'aérologie, CH-1530 Payerne, Switzerland

[3] Laboratory of Radiochemistry and Environmental Chemistry, Paul Scherrer Institute, CH-5232 Villigen PSI, Switzerland

[4] Laboratory for Air Pollution/Environmental Technology, Swiss Federal Laboratories for Materials Science and Technology (Empa), CH-8600 Dübendorf, Switzerland

Abstract

Among the worldwide existing long-term aerosol monitoring sites, the Jungfraujoch (JFJ) belongs to the category where both free tropospheric (FT) conditions and influence from planetary boundary layer (PBL) injections can be observed. Thus, it is possible to characterize free tropospheric aerosol as well as the effects of vertical transport of more polluted air from the PBL. This paper summarizes the current knowledge of the key properties for the JFJ aerosol, gained from the large number of *in-situ* studies from more than 20 years of aerosol measurements at the site. This includes physical, chemical and optical aerosol properties as well as aerosol-cloud interactions and cloud characteristics. It is illustrated that the aerosol size distribution and the aerosol chemical composition are fairly constant in time due to the long distance from aerosol sources, and that many climate relevant aerosol properties can be derived due to this behavior.

Keywords: Mountain Site; Aerosol physical properties; Aerosol optical properties; Aerosol chemical properties; Aerosol-cloud interactions

[*] Corresponding author. Tel: 41-56-310-2465; Fax: 41-56-310-4525

E-*mail address*: nicolas.bukowiecki@psi.ch

[†]Now at: Department of Environmental Science and Analytical Chemistry & Bolin Centre for Climate Research, Stockholm University, Stockholm, Sweden

[‡]Now at: Institute for Aerosol and Sensor Technology, University of Applied Sciences, Windisch, Switzerland.

INTRODUCTION: HISTORY OF AEROSOL MEASUREMENTS AT THE JUNGFRAUJOCH

The High Altitude Research Station Jungfraujoch (3580 m a.s.l., 46°32' N 7°59' E, http://maps.google.com/maps?q=46.547610,7.978979&ll=46.547610,7.978979&z=7), hereafter abbreviated as JFJ (see list of abbreviations at the end of this review), was founded in 1930 (http://www.hfsjg.ch) and is located on an exposed anticline in the Swiss Alps (see Fig. 1a). First sporadic aerosol research activities took place at the JFJ in the early 1970s to investigate the chemical composition of the aerosol at the JFJ (Dams and de Jonge, 1976; Adams *et al.*, 1980). At the same time (1973), semi-continuous measurements of the total mass concentration (total suspended particles, TSP) and particulate sulfate started in support of international research programs focusing on long-range transport and acid rain issues. In 1978, these measurements became part of the Swiss National Air Pollution Monitoring Network (Gehrig *et al.*, 1986). First continuous aerosol measurements with 30-min time resolution were initiated in 1986 using an epiphaniometer (Gäggeler *et al.*, 1989; Baltensperger *et al.*, 1991). In 1995, MeteoSwiss established a Swiss contribution to the Global Atmosphere Watch (GAW) program of the World Meteorological Organization (WMO). This program included an aerosol component, with a wide variety of variables being measured since then, as listed in Table 1.

To provide an overview of the available long-term data, Fig. 1 shows the temporal evolution of various aerosol parameters continuously measured for at least 20 years. These continuous measurements have been highly useful for the detection of recurring and singular aerosol transport events. At the JFJ this is exemplified by the detection of Saharan dust events (Schwikowski *et al.*, 1998; Collaud Coen *et al.*, 2004), by the observation of the remainders of a forest fire in the US (Petzold *et al.*, 2007) or by the characterization of aerosol properties within the volcanic aerosol plume from the eruption of the Ejyafjallajökull volcano in 2010 (Bukowiecki *et al.*, 2010). The operational measurements also provide a vital basis for intermittent intensive measurement campaigns with international participation. The Cloud and Aerosol Characterization Experiments (CLACE), initiated in 2000, still focus on in-depth aerosol characterization, cloud microphysics, and aerosol-cloud interactions.

Among the worldwide existing long-term aerosol monitoring sites, the JFJ belongs to the category where both free tropospheric (FT) conditions and influences from planetary boundary layer (PBL) injections can be observed. Thus, it is possible to characterize free tropospheric aerosol as well as the effects of vertical transport of more polluted air from the PBL. This review summarizes the current knowledge of the key properties of the JFJ aerosol, gained from the large number of in-situ studies (more than 100 peer-reviewed publications at the time of appearance of this article). Columnar optical aerosol properties (AOD), gas phase measurements as well as

remote sensing studies performed at the JFJ (for the investigation of the troposphere further above the site) are discussed in the context of the in-situ measurements but are not in the focus of this overview.

THE ORIGIN OF THE AEROSOL MEASURED AT THE JFJ

Henne *et al.* (2010) recently classified the JFJ as being *mostly remote*. Due to its remote location there are only a few local sources influencing the aerosol at the JFJ. Instead, aerosol variability is for the most part dominated by meteorology-driven transport, namely by the degree of vertical mixing and cloud presence along the air mass trajectory (see next section). Long-range transports such as the special but still frequent cases of Saharan dust events (SDE) are also important regarding various aerosol properties. SDE occur quite frequently at the JFJ, in extreme cases resulting in PM10 mass concentration (mass concentration of particles with an aerodynamic diameter < 10 µm) of up to ~100 µg m^{-3} and reddish dust deposits on the glaciers. These events can be reliably detected via the aerosol optical properties, as described later in this article (Section "Aerosol Optical Properties").

As a result, a large part of the aerosol studies related to the JFJ divide their data in three main categories, i.e. free tropospheric conditions, PBL-influenced, and SDE, although a clear separation between these categories is not always straightforward. Further divisions are often

84 done by horizontal wind direction or source area as well as effects of clouds and wet removal.
85 Accordingly, these classifications will also be used in this overview.

86 In addition to the above, new particle formation events near or at the Jungfraujoch are regularly
87 observed (Nyeki *et al.*, 1999; Burtscher *et al.*, 2001; Weingartner *et al.*, 1999; Nessler *et al.*,
88 2003; Boulon *et al.* 2010; Manninen *et al.*, 2010; Herrmann *et al.* 2015). They are estimated to
89 occur approximately 15% of the time (Herrmann *et al.* 2015), very similar to the frequency
90 within the European PBL (Manninen *et al.*, 2010). Due to their small diameter (<~20 nm), the
91 nucleation mode particles hardly influence bulk aerosol properties except for the particle number
92 concentration. Boulon *et al.* (2010) showed that newly formed particles are correlated with UV
93 but not with calculated H_2SO_4 and concluded that organics are likely to be involved in the initial
94 stages of new particle formation. The same study also found an increased concentration of
95 precursor clusters in air masses arriving from Eastern Europe.

96 Apart from the PBL and long-range transported aerosols, emissions from local activities
97 influence the observed aerosol properties at times. These emissions are either directly caused by
98 the tourists visiting the JFJ, e.g. tobacco smoke, or they are associated with the touristic
99 infrastructure, e.g. helicopter flights, cooking, snowcat driving as well as occasional rock drilling.
100 Snowcat driving and other local combustion sources are clearly seen in black carbon
101 measurements, while helicopter emissions are primarily seen in the particle number concentration

(Baltensperger *et al.*, 1997). Furthermore the presence of lead in the JFJ aerosol has been attributed to leaded fuel used by helicopters and small planes (Worringen *et al.*, 2014), although Cziczo *et al.* (2009) hypothesized that these lead-containing particles rather originate from the free-tropospheric background. The most regular local pollution source, however, is tobacco smoke (first discussed by Morrical *et al.*, 2002, recently also described by Fröhlich *et al.*, 2015). While frequently seen, the local emissions usually have a limited influence on mean values of most aerosol properties. Nevertheless, filtering and flagging are main components of the quality control procedures before delivery to data centers.

FREE TROPOSPHERIC VS. PLANETARY BOUNDARY LAYER INFLUENCED AEROSOL

The presence of PBL-influenced air at the JFJ is the result of manifold meteorological processes taking place over complex terrain both on very local but also larger scale spatial levels. Uplifting of PBL air to the JFJ is mainly driven by convective PBL growth processes and mountain venting (Nyeki *et al.* 2000; Henne *et al.* 2005; Collaud Coen *et al.* 2011; Ketterer *et al.* 2014), but elevated aerosol layers are also transported to the site by advection (Nyeki *et al.* 2002; Collaud Coen *et al.* 2011). More specifically, the PBL over the Swiss plateau (a region of lower altitude north of JFJ surrounded by the Alps to the south and by the Jura mountains to the north-

west) is advected to the Jungfraujoch with north-westerly winds. During this process, the PBL air over the Swiss plateau is transported upwards by slope winds to the JFJ and is mixed with free tropospheric air (Collaud Coen *et al.*, 2011). For cloud-free cases, this has been found to occur if the PBL over the Swiss plateau is higher than 2,800 m a.s.l. (Ketterer *et al.,* 2014). In contrast, the JFJ is influenced by a PBL which is formed over the inner Alpine area and advected to the site during conditions with south-easterly winds (Lugauer *et al.*, 1998).

The discrimination between FT background and PBL influenced conditions is central for understanding of the observed properties of the JFJ aerosol. Dams and De Jonge (1976) found a clear seasonal cycle in TSP concentrations, which was attributed to wind-blown dust from the local mountains, while the snow cover was thought to suppress this in winter. This clear seasonal cycle was subsequently confirmed by the continuous TSP observations (e.g. Gehrig, 1986), but it was only a decade later that it was recognized that vertical transport of PBL air masses to the JFJ is responsible for this seasonality (Baltensperger *et al.*, 1991; 1997). This could be confirmed with airborne lidar measurements when transects over the JFJ massive were flown on a summer day (Nyeki *et al.*, 2000; 2002). The distinct seasonality due to the vertical transport is observed for all of the in-situ aerosol parameters (see Fig. 1) and also for the aerosol optical depth (Ingold *et al.*, 2001).

Baltensperger *et al.* (1997) suggested separating FT and PBL influences by selecting certain time periods, i.e. night and early morning from 03:00 to 09:00 (local standard time), to represent FT conditions. This simple classification based on time of day, was used by Nyeki *et al.* (1998b) and Weingartner *et al.* (1999), but it was recognized that this approach was quite coarse due to the complex topography of the Alps. Lugauer *et al.* (1998) showed how the amount of PBL influence at JFJ relates to the synoptic conditions using the routinely available alpine weather statistics (AWS; Schüepp, 1979), a synoptic weather classification system. The link between these weather classes and vertical transport and the effects on diurnal and seasonal cycles of aerosol properties was addressed in further studies (Lugauer *et al.*, 2000 ; Zellweger *et al.* 2000 ; Kammermann *et al.*, 2010 ; Collaud Coen *et al.*, 2011). However, the AWS classification is purely qualitative and only provides the likelihood of PBL influence.

Using tracers for transport promises a better time resolution and more quantitative determination of PBL influence at JFJ. Zellweger *et al.* (2003) found that NO_y/CO, a common tracer for the photochemical age of an air mass, is a suitable parameter to distinguish between free tropospheric conditions and PBL influence. More recently, Griffiths *et al.* (2014) used ^{222}Rn concentrations to quantify the PBL influence. During the last decade, Lagrangian trajectory models such as LAGRANTO and Lagrangian dispersion models such as FLEXPART have been proven to be useful tools to identify the PBL influence and source regions of air pollutants (e.g.

155 Balzani Lööv *et al., 2008;* Sturm *et al., 2013).* Most recently, Herrmann *et al.* (2015) compared
156 the ability of NO_y/CO, ^{222}Rn concentrations, and FLEXPART simulation results to determine
157 PBL influence. As expected, none of them works perfectly well on a single case basis, but on
158 average they all provide consistent results. FT background conditions prevail about 39% of the
159 time, with a maximum over 60% in winter and a minimum of about 20% in summer. PBL
160 influence along the back trajectory most likely happens either within ~24 hours before arriving at
161 the JFJ or then longer than 5 days ago, as vertical transport is much more efficient over the Alps
162 than over flat terrain. Also, Collaud Coen *et al.* (2011) and Ketterer *et al.* (2014) explained the
163 PBL influence during the night by the presence of a residual layer. Herrmann *et al.* (2015) found
164 that the number concentration of accumulation mode particles under FT background conditions is
165 very constant throughout the year, with $N_{>90nm}$ (the number concentration of particles with
166 diameters > 90 nm) ranging between 35 and 50 cm^{-3}. With PBL influence, $N_{>90nm}$ strongly
167 increases. Thus, the number concentration of accumulation mode particles is also a suitable proxy
168 for FT background conditions. Remote sensing with wind profilers or lidars, very common tools
169 for probing vertical mixing and aerosol layering, have only been applied in one study so far in the
170 vicinity of the JFJ (Ketterer *et al.*, 2014).
171

NUMBER CONCENTRATION, SIZE DISTRIBUTION AND BULK CHEMICAL COMPOSITION

The physical and chemical aerosol properties that are primarily relevant for aerosol-climate interactions are the particle number concentration, the aerosol size distribution and the chemical composition, as they determine the aerosol optical properties and the aerosol-cloud interactions of the bulk aerosol. This section presents findings on these three key properties under FT and PBL influenced conditions.

Particle number concentration climatology

Routine total particle number concentration measurements started in 1995; the lower size cut of the condensation particle counters (CPC) was changed from 3 to 10 nm in 1997, see Table 1. The total particle number concentration exhibits a distinct seasonal cycle (Fig. 1e) due to the seasonality of vertical transport as already shown by Nyeki *et al.* (1998b). In summertime, when the typical PBL injections reach the site, the monthly average total number concentrations range between 800 and 1400 cm^{-3} (see Fig. 1 and Table 2). In wintertime when FT conditions dominate, monthly mean number concentrations vary between 200 and 600 cm^{-3}. The total particle number concentration shows considerable temporal variability as it is also influenced by nucleation events. Nucleation mode particles can dominate the total particle number concentration at times;

during strong nucleation events concentrations of $N_{>16nm}$ up to 17'000 cm^{-3} are reached, the vast majority of those being below 25 nm (Herrmann *et al.,* 2015).

Collaud Coen *et al.* (2007) performed a first trend analysis with 10.5 years of available data. They found a marginal increase in total particle number concentration during winter months, tentatively due to a general temperature increase and thus more PBL lifting also in winter, or due to long-range transport related effects. However, no statistically significant trend was found for the entire 1997-2010 period (13 years) by Asmi *et al.* (2013). A significantly decreasing number concentration was only found for June (-2.5% per year), in addition to a slight, insignificant increase (but in line with Collaud Coen *et al.*, 2007) in January and February (+2.5% per year). A possible change in nucleation event frequencies at the JFJ has not been addressed in trend analysis studies so far.

Number size distribution

First aerosol size distribution measurements at the JFJ were performed for a whole year in 1996/1997 with an optical particle size spectrometer (OPSS, Nyeki *et al.*, 1998a,b), followed by 14 months in 1997/1998 (Weingartner *et al.*, 1999) with a scanning mobility particle sizer (SMPS) and continuous SMPS/OPSS measurements since 2008 (see Table 1 for instrument details and references). These studies consistently showed that the number size distribution of the JFJ aerosol most of the time consists of distinct Aitken and accumulation modes (Herrmann *et*

al., 2015). There is of course also a nucleation mode during new particle formation events, however, a substantial portion of that one falls below the lower detection limit of the SMPS applied in the monitoring program. Fig. 2 shows the mean seasonal pattern of the Aitken and accumulation mode properties (multi-modal lognormal fits). The Aitken mode and accumulation mode diameters shown in Panel (a) only exhibit a very weak seasonality. For the 6-year measurement period from 2008-2014, the modal diameters of Aitken and accumulation mode were found to be 45 ± 11 nm (mean ± 1 standard deviation) and 135±26 nm, respectively (Herrmann *et al.*, 2015). This is in good agreement with those observed by Weingartner *et al.* (1999) during the measurements in 1997/98.

Similar to the total number concentration in Fig. 1e, the seasonal pattern of the integrated SMPS number concentration (Fig. 2b) is due to the seasonality of the PBL influence (except for somewhat lower values due to higher cut-off diameter of the SMPS compared to the total number concentration measured by the CPC). Furthermore, Herrmann *et al.* (2015) also pointed out a clear Hoppel minimum around 80-90 nm in the number size distributions (Hoppel *et al.*, 1986), indicating that the aerosol arriving at the JFJ typically experienced in-cloud processing during their travel, where particles above this diameter were activated and gained aerosol mass through aqueous phase processes. The observed Hoppel minimum agrees well with the mean activation diameter found for the JFJ aerosol (see Section “Aerosol-cloud interactions”).

Bulk chemical composition

The size segregated chemical bulk composition (TSP and PM1, size cut in accordance with WMO/GAW, 2003 and verified by Streit *et al.*, 2000) has been measured semi-continuously (every 6th day) since 1999 with offline ion chromatography on filter samples (ionic species, see Table 1 for details). The routine filter analyses have been complemented by campaign-wise aerosol mass spectrometer measurements (AMS, Aerodyne Inc.), which provide highly time-resolved composition of non-refractory PM1 components. This section puts a focus on the PM1 mass balance and coarse mode composition at the JFJ, while a separate discussion of carbonaceous matter is provided in the next section due to changing terminologies in the last two decades.

The chemical composition of PM1 at the JFJ has been addressed in several studies (long-term: Henning *et al.,* 2003; Cozic *et al.,* 2008a; short-term: Krivacsy *et al.,* 2001; Choularton *et al.,* 2008; Jimenez *et al.,* 2009; Lanz *et al.,* 2010). The mass concentration of individual species or compound classes largely follows the strong seasonal cycle common to most aerosol variables. The comparison of the results for multiple years, certain seasons or campaigns (Fig. 3a) shows that the observed mass fractions of individual species/compound classes are essentially similar for all studies. This means that the averaged mass fractions vary only a little with season, although some temporal variability is of course observed (e.g. Sjogren *et al.,* 2008; Juranyi *et al.,*

2010). In Fig. 3b, the results from the studies included in Fig. 3a are aggregated to a representative average of the PM1 composition. Organic matter dominates with ~50% mass fraction, followed by sulfate (~23%), ammonium (~14%), nitrate (~8%) and BC (~4%). The low BC mass fraction is typical for aged aerosol and the inorganic to organic ratio falls within the typical range of values observed around the globe (Jimenez *et al.*, 2009). Cozic *et al.* (2008a) investigated the ion balance for sulfate, nitrate and ammonium for the filter samples and AMS measurements and concluded that generally the sulfate and nitrate were neutralized by ammonia. Nevertheless, the nitrate to sulfate ratio is much lower than in the PBL, due to the strong vertical gradient of ammonia in the troposphere (Lanz *et al.*, 2010), and occasionally, especially at low concentrations with a usually higher FT influence, the ammonia concentration is not even sufficient to fully neutralize the sulfuric acid (Cozic *et al.*, 2008a). The same is also noticed in the hygroscopicity measurements (see below, e.g. Sjogren *et al.*, 2008). Among the inorganic species, Henning *et al.* (2003) and Cozic *et al.* (2008a) found no significant temporal evolution other than the dominating seasonal cycle caused by the PBL influence.

PM1 contributes about 63% to TSP on average, while the remaining 37% are contributed by the coarse mode (measurement period 2004-2007, Cozic *et al.*, 2008a). The composition of the coarse mode is dominated by mineral components due to Saharan dust and dust from the rocks around the JFJ (e.g. Streit *et al.*, 2000). Calcium and nitrate are the only species with a significant

contribution to the coarse mode among those covered by the long-term ion measurements (Henning *et al.*, 2003; Cozic *et al.*, 2008a). The studies hypothesize that nitrate is linked with calcium in the coarse mode by the reaction of mineral dust particles with nitric acid to form $Ca(NO_3)_2$. Other coarse mode compounds relevant for a mass balance have not been regularly measured (e.g. silica).

During SDE events, the coarse mode gives the dominant contribution to TSP and its composition is dominated by that of aged Saharan dust. Collaud Coen *et al.* (2004) showed through elemental analysis of filter and ice core samples from JFJ that the concentrations of magnesium, calcium and potassium were significantly enhanced during SDE. All these components are actually constituents of illite and montmorillonite. Additionally, Grobéty *et al.* (2011) found that most of the SDE particles are clay minerals, which contain attachments or inclusions of hematite (Fe_2O_3) and rutile (TiO_2) with diameters between 40 - 200 nm.

The volatility of the bulk aerosol at the JFJ has only been addressed in a few studies so far. Burtscher *et al.* (2001) applied a thermodesorber downstream of an SMPS during a nucleation burst. About 90% of nucleation mode particles in the diameter range 19-25 nm evaporated at $T <$ 125 °C. This is in contrast to larger particles, which are characterized by a much lower volatility: 40, 60 and 88 % of the SMPS volume measured at 30 °C volatilized after exposure to 125, 175 and 275 °C, respectively. In another study, Nessler *et al.* (2003) found that 28% of particles < 100

nm evaporated when comparing ambient (ambient temperature and relative humidity) to dry (laboratory temperature and relative humidity) SMPS size distributions. At the same time, dry number size distributions were shifted to slightly lower diameters, mostly due to the loss of water.

Carbonaceous matter

Carbonaceous aerosol comprises organic matter and black carbon. The black carbon mass concentration has continuously been measured at the JFJ since 1995 by aethalometers (AE10 and AE31) and since 2003 also by a multi-angle absorption photometer (MAAP, see Table 1). Both methods only provide "equivalent black carbon" mass concentrations (see Petzold *et al.*, 2013 for BC related terminology), as the BC mass is inferred from the light absorption measurements using a mass absorption cross section (MAC). Cozic *et al.* (2007) determined the site specific MAC value by relating the absorption coefficient measured by the MAAP with the mass concentration of elemental carbon (EC) determined with a thermal optical method (Sunset ECOC analyzer; EUSAAR-2 protocol, Cavalli *et al.*, 2010). For winter and summer they found MAC values of 7.6 $m^2\ g^{-1}$ and 11 $m^2\ g^{-1}$ (for BC at λ = 637 nm), respectively. Weingartner *et al.* (2003) and Collaud Coen *et al.* (2010) used aethalometer and MAAP data sets to develop new data analysis algorithms to correctly infer the absorption coefficient from aethalometer raw data. This also ensures that older BC data derived from the AE31 can be tied to the MAAP time series in a

297 homogeneous manner. For the AE10, the instrument and site-specific conversion factor was
298 determined by Lavanchy *et al.* (1999).

299 Liu *et al.* (2010) characterized BC at the JFJ using a Single Particle Soot Photometer (SP2). By
300 comparison against the MAAP they determined a MAC value of ~10.2 m^2 g^{-1} (at λ = 637 nm),
301 which is consistent with above results. They also showed that ~40% of the BC particles are
302 internally mixed with large amounts of other aerosol components. However, this fraction is a
303 lower limit for the degree of internal mixing as it did not include BC particles with moderate
304 coatings.

305 Most studies investigating the organic matter at the JFJ applied thermal optical methods or an
306 AMS. Krivacsy *et al.* (2001) showed with thermal optical methods that for a summer case about
307 half of the organic species (within PM2.5) were water soluble. Furthermore, the comparison of
308 thermal-optical methods to an AMS for the wintertime aerosol provided an organic matter to
309 organic carbon ratio of OM/OC = 1.8 (Cozic *et al.*, 2008a), which is consistent with the O:C
310 (oxygen to carbon) ratio of 0.5 determined by Jimenez *et al.*, (2009) from the mass spectrum.
311 These values are typical for a highly oxidized and photochemically aged aerosol as already
312 shown in a qualitative manner by Alfarra *et al.* (2006). Lanz *et al.* (2010) also found a low
313 volatility for the oxygenized fraction of the organic aerosol at the JFJ. In 2012/2013 14 months of
314 ToF-ACSM (time-of-flight aerosol chemical speciation monitor; Fröhlich *et al.,* 2013)

315 measurements were performed. This allowed for a more advanced analysis of the sources of the
316 organic aerosol (Fröhlich *et al., 2015*). The organic aerosol was during all seasons dominated by
317 oxygenated organic aerosol (71–88 %), but also showed contributions from local tourism-related
318 activities (e.g. tobacco smoke, 7–12 %) and hydrocarbon-like organic aerosol related to regional
319 vertical transport (3–15 9%).
320

321 AEROSOL OPTICAL PROPERTIES

322 *Climatology of aerosol optical properties*

323 The aerosol scattering coefficient and all derived optical aerosol properties strongly depend on
324 the aerosol size distribution, because the scattering cross section is approximately proportional to
325 the aerosol surface area concentration. At the JFJ the accumulation mode particles dominate the
326 aerosol surface distribution (mode diameter between 200 and 250 nm, Weingartner *et al.,* 1999).
327 Therefore the aerosol scattering coefficient measured by the nephelometer (Table 1) is sensitive
328 to changes in the accumulation mode and comparably insensitive to ultrafine and coarse mode
329 particles (except for SDE episodes, see Zieger *et al.*, 2012). Furthermore, the scattering
330 coefficient is also wavelength dependent. The scattering Ångström exponent, $å_{sp}$, is a useful
331 quantity since it is a qualitative indicator of the particle size distribution. Aerosols dominated by

332 the coarse mode (d >1 µm) have small exponents ($å_{sp}$<1), whereas aerosols dominated by the fine
333 mode (d <1 µm) have large values ($å_{sp}$ >2).

334 In contrast, the aerosol absorption coefficient is approximately proportional to the amount of
335 light absorbing species. Despite being a minor species (~4% of PM1, see Section "Bulk chemical
336 composition"), the dominant contribution to light absorption comes from BC, which is a very
337 strong light absorber. Saharan dust is a much weaker light absorber; however, it can give a
338 substantial contribution to light absorption during SDE events (see Table 2), when it is
339 dominating the mass of the aerosol (Collaud Coen *et al.*, 2004).

340 Both the absorption and the scattering coefficients again show a climatology similar to the
341 particle number concentration, with low values in winter and high values in summer (see above).
342 Collaud Coen *et al.* (2013) performed a trend analysis for the aerosol scattering coefficient (1995-
343 2010) and the aerosol absorption coefficient (2001-2010). In analogy to the total number
344 concentration, no annual statistically significant trend was found for these two parameters either,
345 with the exception of a statistically significant negative trend for the scattering coefficient in
346 August. This is also in-line with a trend analysis for the aerosol optical depth (AOD) above the
347 JFJ for 1995 – 2010 which found no significant trend either (Nyeki *et al.*, 2012).

348 Andrews *et al.* (2011) performed a climatology for aerosol optical properties at mountain top
349 observatories. Fig. 4 shows the seasonal variation at the JFJ of absorption, scattering, extinction,

net radiative forcing as well as for single scattering albedo and the scattering Ångström coefficient, for all available data until 2007. Related to the rather constant composition of the JFJ aerosol, the single scattering albedo and the scattering Ångström exponent show only a minor seasonal variation compared to the other (mainly PBL influenced) parameters. The study also indicated that the JFJ aerosol has a negative radiative forcing efficiency. The results presented by Andrews *et al.* (2011) represent measurements under dry conditions for better comparability to other stations (as recommended by WMO/GAW, 2003). For a comparison with satellite data and for net radiative forcing estimates, the scattering coefficient and all derived parameters need to be corrected for the scattering enhancement due to water uptake at ambient relative humidity (see section "The effect of water uptake on the aerosol optical properties").

Detection of Saharan dust

Since 2001 both the absorption and the scattering coefficients have been measured at several wavelengths, which allows studying the single scattering albedo (SSA) wavelength dependence (expressed by the Ångström exponent of the SSA, $å_{SSA}$). In the presence of Saharan mineral dust particles, an inversion of the SSA wavelength dependence is observed (Collaud Coen *et al.*, 2004). This can be attributed to two peculiar properties of Saharan dust: large particle sizes extending into the coarse mode (resulting in a lower than normal Ångström scattering coefficient) and light absorption in the visible wavelength range due to hematite inclusions in the dust

368 particles (resulting in a higher than normal Ångström absorption coefficient). SDE are therefore
369 automatically detected at the JFJ by the occurrence of negative $å_{SSA}$ that last during more than 4
370 hours, and an alert sent by e-mails is currently available. Collaud Coen *et al.* (2004) validated this
371 SDE detection method by either filter coloration, back-trajectory analysis, satellite measurements
372 or a combination of these methods. It is now an accepted method which is corroborated by lidar
373 and ceilometers, AOD, size distribution and chemical measurements. The analysis of a peculiar
374 SDE during the summer CLACE 2010 campaign (Zieger *et al.*, 2012) has however shown that
375 the presence of coarse mode particles in the size distribution measurements (SMPS and OPSS) is
376 more sensitive for the detection of SDE than $å_{SSA}$, because with the latter method periods with
377 SDE influence can be missed due to an enlarged fine mode during PBL influence. This
378 phenomenon is probably more important in summer, when the PBL influence is the greatest.
379 The 2001-2014 SDE climatology (Fig. 5) shows the highest SDE probability in the late spring
380 (May, June) and autumn (mainly October). Based on trajectory analyses, the traveling time of the
381 dust plumes was on average about 100 hours, with most of the SDE being transported from
382 southerly directions to the JFJ in 2 days. Extremely long transport times up to 13 days arriving
383 from Northeast are however also observed (Collaud Coen *et al.*, 2004; Thévenon *et al.*, 2012).
384 The most important potential source countries were situated in the north-western and north-
385 central parts of the Sahara desert (Algeria, but also Morocco, Libya, Tunisia, and Mali).

AEROSOL HYGROSCOPICITY AND CCN ACTIVITY

Hygroscopic particle growth

The hygroscopicity describes the ability of atmospheric aerosol particles to absorb water at elevated relative humidity (RH). The associated growth of the particles influences how strongly many aerosol parameters vary with variations of ambient RH and how readily a particle acts as a cloud condensation nucleus. Aerosol hygroscopicity at subsaturated RH was studied at the JFJ with a hygroscopicity tandem differential mobility analyzer (HTDMA). This instrument determines the growth factor (GF), which is defined as the ratio of the particle diameter at a given relative humidity to the dry particle diameter. HTDMA measurements in different studies at the JFJ were either performed approximately at ambient temperature (-10 °C in winter and 0.5 °C in summer) in order to avoid potential evaporation losses of semi-volatile aerosol components (Weingartner *et al*., 2002; Sjogren *et al*., 2008), or at room temperature (~25 °C; Sjogren *et al*., 2008; Kammermann *et al*., 2010). However, no significant differences in aerosol hygroscopic properties were observed between the ambient and room temperature measurements (Sjogren *et al*., 2008; Kammermann *et al*., 2010). This is in line with the fact that no major fraction of highly volatile material is present in the particle diameter range above 50 nm (by Burtscher *et al*., 2001; Nessler *et al*., 2003).

Growth factors for different particle dry diameters from the individual studies are shown in Table 2. Kammermann *et al.* (2010) did not observe a distinct seasonal pattern, which again is consistent with the absence of a clear seasonal pattern in the bulk chemical composition. The annual mean growth factors at RH = 90 % are 1.35, 1.46 and 1.51 at the dry diameters of 50, 110 and 265 nm, respectively, where the size dependence is mainly caused by the decreasing influence of the Kelvin effect for increasing size rather than by distinct changes in the chemical composition (see next section). These long-term measurements largely confirmed results from the earlier short-term studies by Weingartner *et al.* (2002) and Sjogren *et al.* (2008).

The hygroscopic growth factor of a particle depends on the RH and, for substances that show hysteresis behavior, also on the RH history. Measurements of hydration and dehydration cycles revealed that no hysteresis with distinct deliquescence or efflorescence transitions occurred for the JFJ aerosol (Weingartner *et al.,* 2002; Sjogren *et al.,* 2008). This is in contrast to the behavior of many pure inorganic salts and can possibly be explained by the fact that the particles are internal mixtures of multiple salts and organic matter.

HTDMA measurements also provide insights into the mixing state of the aerosol. Sjogren *et al.* (2008) showed that the JFJ aerosol is often largely internally mixed, which is not surprising for aged aerosols. Special cases are Saharan dust events, when externally mixed non-hygroscopic particles can be observed at the larger sizes (Sjogren *et al.*, 2008). However, the long-term data

set from Kammermann *et al.* (2010), which is included in Table 2, reveal that the growth factors in the Aitken and accumulation mode range are largely unaffected by the presence of Saharan dust, with the exception of a slightly increased fraction of non-hygroscopic particles and a slightly decreased 10^{th} percentile level of the mean GF for the 265 nm particles compared to the non-Saharan-dust periods (not shown here). This confirms that the Saharan dust events detected at the JFJ do not have a significant influence on aerosol fine mode particle number concentration in most cases, despite their high dust mass concentrations. However, this does not apply for the RH-dependence of optical properties, as will be shown below.

The hygroscopicity parameter* κ *and closure studies

The hygroscopic growth of aerosol particles and their CCN activation behavior is described by Köhler theory (e.g. McFiggans *et al.*, 2006), which accounts for the Raoult and Kelvin effects. Petters and Kreidenweis (2007) introduced the simplified κ-Köhler theory, in which the Raoult term is captured with a single hygroscopicity parameter κ. The κ-value is widely used, on the one hand for comparing hygroscopicity measurements made with different methods at different RH, or closure studies, and on the other hand, whenever a simple description of the aerosol hygroscopic and CCN activation behavior is required such as e.g. box models for cloud microphysics.

439 The κ parameter of the JFJ aerosol was retrieved via the κ -Köhler theory both from HTDMA
440 measurements (Kammermann *et al.*, 2010, see two sections above) and combined CCNC/SMPS
441 measurements (Jurányi *et al.*, 2011, see next section), see Fig. 6. For particles larger than 80 nm
442 in diameter, the κ values for the two different methods and all classifications (by season, free
443 troposphere and Saharan dust events) fall into a narrow range of $\kappa = 0.20 - 0.25$. The small
444 variability of κ makes it possible to describe the aerosol hygroscopicity of the accumulation mode
445 aerosol in very good approximation with a single constant number. A consequence of this is that,
446 as shown in the next section, the CCN number concentrations at the JFJ can be estimated with
447 high accuracy based on the measured size distribution with simply using the above averaged κ
448 value of 0.22 (Juranyi *et al.*, 2011).
449 A row of further hygroscopicity closure studies have been performed for the Jungfraujoch
450 aerosol. The close agreement between long-term average κ values derived from HTDMA and
451 CCNC (Fig. 6) was also confirmed for time-resolved data by Juranyi *et al*. (2010). Juranyi *et al.*
452 (2010) showed that on a day-to-day scale, PBL related variations in chemical composition are
453 responsible for observed variations of CCN-derived κ values. Good agreement between
454 composition and growth factor derived κ values for data sets from three CLACE campaigns was
455 shown by Sjogren *et al.* (2008), when assuming a κ value of 0.128 for the organic aerosol
456 components, which is a reasonable assumption when considering the highly-oxidized nature of

457 the organic aerosol components at JFJ (see Section "Carbonaceous matter"). The κ value of the
458 organic aerosol fraction is known to depend on its degree of oxidation. Indeed, Jimenez *et al.*
459 (2009) and Duplissy *et al.* (2011) showed, by comparing HTDMA-derived κ values of the
460 organic aerosol component from smog chamber measurements with ambient data from several
461 sites including JFJ, that the κ value strongly depends on the O:C ratio. Furthermore, they
462 developed parametrizations to infer the κ value of the organic aerosol from its O:C ratio, which is
463 often available from AMS measurements.
464
465 ***CCN measurements and climatology***
466 To investigate the ability of the JFJ aerosol to become activated to cloud droplets, a cloud
467 condensation particle counter (CCNC) has been operational since 2008 (see Table 1 for further
468 reference). The CCN concentration is influenced by the number, the diameter and the chemical
469 composition of the particles. Due to the low total aerosol number concentrations at the JFJ (see
470 Table 2) the number of cloud droplets formed is mainly limited by the number of available CCNs
471 (Hoyle *et al.*, 2015). Fig. 7 shows that at water supersaturations above 1 %, more than 40 % of
472 the aerosol particles at the JFJ are able to act as CCN. In contrast, only 20 % of the aerosol
473 particles may act as CCNs at a supersaturation of 0.2 %. The lower CCN fraction in winter is
474 caused by a higher contribution of Aitken mode particles to the total particle number

concentration during this season, as illustrated in Fig. 2d/2e. The CCN active fraction for the JFJ is much lower compared to many other European sites (Paramonov *et al.,* 2015). This can be explained with the comparably high number fraction of Aitken mode particles at the JFJ.

Analyzing 17 months of CCNC and SMPS data, Jurányi *et al.* (2011) found a very small temporal variability and no seasonal pattern of the critical dry activation diameter at a certain supersaturation. This can be attributed to the small variability of the chemical composition (see Section "Bulk chemical composition"). As a consequence, it is possible to predict the CCN number concentration with high accuracy solely from the measured number size distribution and using a fixed and size-independent hygroscopicity parameter of 0.22 (80 % of all predicted CCN number concentrations of the 17 month period fall within ±25% of the measured value). While it is possible to treat the composition/hygroscopicity in a simplified manner for CCN predictions, the variability of size distribution needs to be taken into account (see Juranyi *et al*., 2010 and 2011, for detailed sensitivity analyses). The CCN number concentration is approximately 5-12 times higher in summer. The major part of this variation is explained by the seasonal amplitude of total particle number concentration (amplitude factor 4.5; Fig. 1), further amplified (factor 1.1-2.6) by the increased accumulation mode fraction in summer (Fig. 2), which causes a higher activated fraction (Fig. 6).

493 ***The effect of water uptake on aerosol optical properties***

494 The water uptake ability of aerosol particles does not only influence their activation properties,
495 but also their optical properties. At the JFJ all in-situ properties are measured at dry conditions
496 (sampling at RH < 20 %). A low RH is recommended by WMO/GAW (2003) to determine
497 aerosol properties at well-defined conditions that are comparable for all stations around the globe.
498 However, this also implies that the dry measured values differ from the ambient and thus climate
499 relevant ones. The scattering enhancement factor f(RH) is the key parameter to describe the RH
500 dependence of the particle light scattering coefficient σ_{sp} and is defined as the ratio of the ambient
501 $\sigma_{sp}(RH_{amb})$ divided by its dry value $\sigma_{sp}(RH_{dry})$. Knowledge of this RH effect is of crucial
502 importance for climate forcing calculations but is also needed for the validation or comparison of
503 remote sensing with in-situ measurements.

504 The f(RH) value depends on the composition, hygroscopicity and size of the particles (as well
505 as on the wavelength). As the variability of composition and hygroscopicity is well defined and
506 rather limited for the JFJ aerosol (see above), the variability of f(RH) is mainly driven by the
507 variability of the size distribution. Thus, Nessler *et al.* (2005a) developed an algorithm that adapts
508 the dry nephelometer measurements of σ_{sp} at the JFJ to ambient conditions. They predicted f(RH)
509 using the measured Ångström exponent of σ_{sp}, which is a crude measure for size and aerosol type
510 (e.g. mineral dust during the SDE) at the JFJ. Later, f(RH) was directly measured at the JFJ for

two observation periods in 2008 (CLACE 2008; Fierz-Schmidhauser *et al.*, 2010b) and 2010 (CLACE 2010; Zieger *et al.*, 2012), using a humidified nephelometer system (WetNeph) developed at PSI (Fierz-Schmidhauser *et al.*, 2010a). The typical FT and PBL influenced aerosol (Fig. 8a) exhibits a gradual rise of f(RH) as a function of RH, without distinct deliquescence or efflorescence transitions during hydration and dehydration, respectively, nor any discernible hysteresis. This is in agreement with the behavior of hygroscopic growth factors discussed above. At RH=80% and λ =550 nm f(RH) typically reaches a value of 2. Exceptions are the periodically observed Saharan dust episodes, when f(RH) consistently remains small to moderate, reaching only a value of ~1.2 at 80% RH (see Fig. 8b). This is a contrast to the hygroscopic growth factors discussed above, on which SDE usually only have very limited effects. It can be explained by the fact that the dust particles give a substantial to dominant contribution to light scattering, while they only give a negligible to minor contribution to particle number in the diameter range below 265 nm covered by the hygroscopic growth factor measurements.

The RH dependence of *f*(RH) can be parameterized in a good approximation by using the following empirical parameterization

$$f(RH) = a(1 - RH)^{-\gamma} \quad (1)$$

where γ describes the magnitude of the enhancement and *a* the intercept at RH=0%. The intercept improves the empirical parameterization of the *f*(RH)-humidograms, however, it should be noted

529 that values of *f*(RH) below 1 are defined to be 1. The distributions of the fit coefficients γ and *a*
530 are shown in Fig. 8c and 8d and are listed in Table 2 for all measured humidograms of the
531 CLACE2010 campaign and beyond (Zieger *et al.*, 2012). The distinct bimodal feature of both
532 distributions can be explained by the occurrence of two distinct aerosol types: in most cases, in
533 the absence of Saharan dust influence, a hygroscopic aerosol with γ between around 0.3 and 0.7
534 or, less frequently, Saharan dust dominated aerosol with low hygroscopicity, i.e. with γ between
535 around 0.0 and 0.2. This clear discrimination between two aerosol types only makes a prediction
536 of *f*(RH) at the JFJ rather simple, as SDE events can be identified from the measured dry aerosol
537 optical properties alone (see above). This "simple" behavior of the FT aerosol is in contrast to
538 that at more polluted sites with more variable aerosol properties, where further information on the
539 particle size distribution and the main chemical composition of fine and coarse mode is needed to
540 infer the *f*(RH) in good approximation (Zieger *et al.*, 2013).
541 Nessler *et al.* (2005b) also performed a theoretical sensitivity analysis to investigate potential
542 light *absorption* enhancement at elevated RH. Absorption enhancement effects due to absorption
543 of water on coated BC particles are expected to be very small due to compensating effects of
544 increasing coating thickness and decreasing index of refraction of the coating. A maximal
545 influence of 0.2% on the SSA due to absorption enhancement was found, because at the JFJ the

scattering enhancement is by far larger than the absorption enhancement and the aerosol extinction is dominated by the particle light scattering.

Recalculation of dry aerosol optical properties to ambient RH, using the f(RH) values from above, is needed for correct assessment of the aerosol radiation interactions, but also when comparing remote sensing of aerosol optical properties to dry in-situ measurements. The latter has been done during the CLACE2010 campaign, when an aerosol lidar (light detection and ranging) was operated below the Jungfraujoch at Kleine Scheidegg with the tilted laser beam pointing towards the station. Zieger *et al.* (2012) found good agreement between lidar and RH-corrected in-situ particle light extinction coefficients. However, the quality of the agreement was influenced by orographically produced cloud patches surrounding the JFJ.

AEROSOL CLOUD INTERACTIONS

Cloud presence at the JFJ

Due to its altitude and location the JFJ is regularly engulfed in clouds. In summer, convective clouds are regularly formed in the afternoon along the steep mountain faces northwest of the site (see Fig. 1a) and are then transported towards the site and the surrounding summits. The formation of these clouds is usually characterized by a high updraft velocity of the air mass. In contrast, a relatively stationary and spatially well-defined cloud cap engulfing the JFJ is regularly

564 observed during strong Foehn wind conditions from the Southeast (see e.g. Zieger *et al.,* 2012).
565 Due to the flatter terrain South of the JFJ formed by the Great Aletsch Glacier (Fig. 1a), the
566 formation of this cloud cap is associated with lower air mass updraft velocities. Additionally, the
567 site is directly reached by advective clouds during low pressure situations all year round.

568 On average, the site has been found to be in clouds 40% of the time. This was first estimated
569 by Baltensperger *et al.* (1998) and was recently verified by Herrmann *et al.* (2015), who
570 estimated the cloud presence at the site for a multiannual period from the sky temperature, from
571 the relative humidity as well as from webcam pictures.

572 ***Formation of cloud droplets and ice crystals***

573 While liquid clouds dominate the summer months, mixed-phase and glaciated clouds are
574 present during the rest of the year. With a combination of two different aerosol inlets (a heated
575 *total* inlet sampling all aerosol particles plus an *interstitial* inlet removing the cloud droplets) the
576 interstitial aerosol and the total aerosol can be separated to derive the fraction that was activated
577 to cloud droplets. This experimental setup has also been shown to discriminate between different
578 cloud phases and has been applied and described in a long list of studies (e.g. Henning *et al.,*
579 2002; Cozic *et al.,* 2007; Verheggen *et al.,* 2007; Choularton *et al.,* 2008; Hammer *et al.,* 2014a).
580 From size distribution measurements behind these inlets the scavenging ratio as a function of
581 particle diameter (i.e. an activation curve) can be determined. Fig. 9 shows example activation

curves for different cloud types. For fully liquid clouds, the scavenging ratio reaches 1, indicating that above the activation diameter (which may vary for aerosols with different chemical composition) all aerosol particles are scavenged into cloud droplets. In case of entrainment of dry air into the cloud (as often during Foehn wind conditions at the JFJ), cloud droplets again evaporate and are released to the interstitial aerosol phase. This results in a lower plateau value in the activation curve. Finally, activation curves for mixed phase and fully glaciated clouds are characterized by very low plateau values or simply a zero line. This is due to the Wegener-Bergeron-Findeisen process, which causes an efficient water transfer from the liquid to the ice phase and thus releases the CCNs to the interstitial phase (Baltensperger, 2010, and references therein).

A more quantitative parameter to describe aerosol partitioning into the cloud phase is the activated fraction of particles larger than 100 nm in diameter, $AF_{>100}$. This parameter can be taken as a simplified proxy for the number fraction of liquid cloud droplets in mixed-phase clouds. Henning *et al.* (2004) and Verheggen *et al.* (2007) showed that already an ice mass fraction of 0.1 is sufficient to decrease $AF_{>100}$ down to 0.1, illustrating the effectiveness of the Wegener-Bergeron-Findeisen process. The studies also show that at the JFJ, the activated fraction is 0.5 or lower for ambient temperatures lower than -5 °C.

Characterization of liquid clouds

Liquid clouds form at the JFJ in the temperature range above ~5 °C (Verheggen *et al.*, 2007). The liquid water content (LWC), along with the vertical depth of the cloud, can be taken as a measure for the cloud optical thickness. The in-situ measurements performed in liquid clouds at the JFJ (Baltensperger *et al.*, 1998; Henning *et al.*, 2002; Hammer *et al.*, 2014a) yielded LWC values in the range 0.15 to 0.6 g m^{-3} (for stable cloud conditions only). At a given LWC, the optical thickness also depends on the cloud droplet number concentration. Henning *et al.* (2002) showed for persistent cloud conditions that the threshold dry diameter, separating the smaller particles that remained interstitial from larger particles that were activated to cloud droplets, was largely independent of LWC. Thus, the droplet size for a given LWC is anticorrelated with the available CCN number concentration. Campaign-wise measurements using optical spectrometers reported an average liquid cloud droplet diameter around 10 µm (Henning *et al.*, 2002; Hammer *et al.*, 2014a; Spiegel *et al.*, 2012; Henneberger *et al.*, 2013).

Whether or not a particle forms a cloud droplet depends on its CCN properties, i.e. dry diameter and hygroscopicity (see above), but also on the peak supersaturation in the cloud, which in turn depends on updraft and aerosol feedbacks. Hammer *et al.* (2014a) analyzed in-situ aerosol-cloud interaction measurements from 5 summer campaigns between 2000 and 2011 in order to determine the threshold diameter for droplet activation. They found a rather constant dry

618 activation threshold diameter with an overall median of 87 nm (Table 2). As the CCN properties
619 of the aerosol are well-characterized (see above), it is possible to infer the effective peak
620 supersaturation in the cloud from the observed activation threshold diameter. Using this
621 approach, Hammer *et al.* (2014a) retrieved a median peak supersaturation of 0.35 % for the liquid
622 clouds encountered at JFJ (Table 2). The observed activation threshold diameters and
623 consequently also the inferred cloud peak supersaturations were systematically different for local
624 wind from the northwestern sector (peak supersaturation = 0.41%) compared to the southeastern
625 sector (peak supersaturation = 0.22%). This could be attributed to orographic differences and to
626 the dominating influence of the air mass updraft velocity (Hammer *et al.,* 2014a,b). The slopes on
627 the southeastern side are shallower than those on the northwestern side, thus resulting in lower
628 updraft, lower peak supersaturation and higher activation threshold dry diameter.

629 Secondary aerosol formation through heterogeneous oxidation of precursor gases in cloud
630 droplets, such as e.g. sulfur dioxide to sulfate conversion, is a well-established process. Also for
631 the JFJ, Herrmann *et al.* (2015) showed a clear Hoppel minimum around 80-90 nm in the number
632 size distributions (see Section "Number size distributions"), corresponding well with the
633 observed mean activation diameter. Chemical analysis of cloud water and CCNs at the JFJ indeed
634 confirmed an increased sulfate concentration compared to the background aerosol due to in-cloud
635 processing of sulfur dioxide (Baltensperger *et al.,* 1998; Kamphus *et al.,* 2010). Cloud processing

636 also results in an internal mixture of organics, sulfate and nitrate (Choularton *et al.*, 2008;
637 Targino *et al.*, 2009).

638 ***Characterization of mixed phase and glaciated clouds***

639 Similar to cloud droplets, ice crystals in mixed phase and glaciated clouds at the JFJ are only
640 formed heterogeneously (for temperatures above -38°C). Here, aerosol particles act as ice
641 nucleating particles (INP) by coming into contact with supercooled cloud droplets (contact
642 freezing), or by initiating freezing from within a cloud droplet by immersion or condensation
643 freezing, or by acting as deposition nuclei. Contact freezing is usually the most efficient process
644 at slight supercooling, while at lower temperatures immersion freezing can be more prevalent
645 (e.g. Lohmann and Diehl, 2006).

646 The fact that different modes of ice nucleation exist makes the characterization of INP in the
647 field difficult. Also, compared to CCN, particles that are able to act as ice nuclei are present at
648 much lower concentrations. As a result, the field characterization of INP and ice residual particles
649 (IRP) needs an entirely different approach of investigation compared to liquid cloud studies, both
650 with respect to ice crystal separation and INP characterization.

651 At the JFJ, ice nucleating particles and ice residual particles have been investigated in a row of
652 intensive measurement campaigns since 2000. Ice crystal sampling and separation has been
653 achieved based on a counterflow virtual impactor (Mertes *et al.*, 2007) and recently based on a

654 droplet evaporation tube that makes use of the Wegener-Bergeron-Findeisen process
655 (Kupiszewski *et al.*, 2015). The ice residual particles were subsequently analyzed by a long list of
656 both bulk analysis and single particle analysis techniques, as discussed hereafter. Ice crystals
657 were also directly sampled at ambient conditions and analyzed by imaging techniques
658 (Henneberger *et al.*, 2013). The ice nucleating particle concentrations measured during the
659 performed studies ranged from < 3 L^{-1} (Bundke *et al.*, 2011) up to 14 L^{-1} (Chou *et al.*, 2011).

660 Also for ice nucleating particles, their size has a relevant influence on their ice forming
661 behavior. Ehrman *et al.* (2001) observed an enrichment of coarse mode ice nucleating particles in
662 small ice crystals sampled at the JFJ. Mertes *et al.* (2007) found that the ice nucleation efficiency
663 increases with particle size. However, since the number concentration of aerosol particles drops
664 steeply with increasing size, the observed ice residual particles are generally dominated by
665 submicron particles. This behavior has been verified in a recent JFJ study (Worringen *et al.*,
666 2014), finding a maximum in the ice residual particle number size distribution at around 400 nm,
667 plus a second maximum at > 1 µm in a few cases. Whether the small ice residuals can be
668 interpreted as atmospheric ice nuclei is an ongoing debate.

669 The available data on the chemical composition of ice residual particles collected at the JFJ
670 point towards a composition that is dominated by mineral components, carbonaceous material
671 (both black carbon and organics) as well as sulfate (Kamphus *et al.*, 2010; Cozic *et al.*, 2008b,

672 Targino *et al.*, 2008; Ebert *et al*,. 2011; Worringen *et al.*, 2014). Cozic *et al.* (2008b) found an
673 enrichment of black carbon mass in the ice residual particles (bulk aerosol: 3% BC, ice residuals:
674 27% BC). Saharan dust particles become dominant ice nucleating particles during respective
675 events at the JFJ (Kamphus *et al.*, 2010). Ebert (2011) hypothesized that most ice nucleating
676 particles at the JFJ are internal mixtures containing anthropogenic components and that an
677 admixture of anthropogenic components (like soot) enhances the ice nucleating efficiency.
678 To investigate the ability of the JFJ aerosol to act as ice nuclei, Chou *et al.* (2011) exposed the
679 total aerosol to deposition nucleation freezing and found ice nucleation particle number
680 concentrations between 8 L^{-1} in March and 14 L^{-1} in June. The results from a longer term study
681 using the same technique (Kanji *et al.*, 2014) show a range of 0.1 to 1 L^{-1} for winter and 10 -100
682 L^{-1} in summer, plus around 500 L^{-1} during strong Saharan dust influence. Conen *et al.* (2014)
683 performed an analogous climatology for the immersion freezing potential (at -8 °C) of the JFJ
684 aerosol. They found respective ice nucleation particle concentrations between 1 and 10 L^{-1} in
685 winter and up to more than 1000 L^{-1} in summer and speculate that these very abundant ice nuclei
686 at the site during summer originate rather from fertile regions in Europe and not from Saharan
687 dust plumes or their remainders.
688

THE RELEVANCE AND ROLE OF THE JFJ AEROSOL PROPERTIES IN INTERCOMPARISON AND MODEL STUDIES

The aerosol data measured at the JFJ has been used in numerous intercomparisons and model studies. In comparison to other sites, the JFJ size distribution has clearly been characterized to be a typical sink size distribution (van Dingenen *et al.,* 2004; Beddows *et al.,* 2014). Interestingly, the climatology of new particle formation at the JFJ is not exclusively linked to its altitude, as indicated by Manninen *et al.* (2010) who grouped the new particle formation characteristics at the JFJ together with remote but low altitude stations in Hyytiälä (Finland), Vavihill (Sweden) and Cabauw (Netherlands).

Also the aerosol optical properties are in line with other remote locations at elevated altitude (Andrews *et al.,* 2011). Compared to other aerosol types, the water uptake related scattering enhancement at JFJ is in the intermediate range: located in between very low values observed for highly polluted, mineral dust or organic dominated boreal aerosol and elevated values for maritime and Arctic aerosol (Zieger *et al.*, 2010; 2013).

Due to these characteristics, the JFJ aerosol data have been used as input for a row of modeling studies. The bulk chemical composition (Cozic *et al.,* 2008a) was used as input in a model intercomparison of aerosol-cloud-precipitation interactions in stratiform orographic mixed-phase clouds (Mühlbauer *et al.,* 2010). Van Spracklen *et al.* (2010) and Reddington *et al.* (2011) used

size-resolved particle number concentration data (harmonized by Asmi *et al.*, 2011) to model particle number concentrations on a European scale and on a worldwide level. The same data were also used in an intensive intercomparison of available aerosol size distribution models (Mann *et al.*, 2014). This model intercomparison found that the number concentration at the JFJ can be well predicted by the available models. In a further model study (Hoose *et al.* 2008) the measured relationship between the number of ice crystals, number of aerosols and the ice mass fraction (Verheggen *et al.*, 2007) was used to model the aerosol processing in mixed-phase clouds. A further example is the study by Kristiansen *et al.* (2012) where the coarse mode size distribution at the JFJ after the Eyjafjallajökull eruption in 2010 was used to validate a plume transport model. The diurnal development of the PBL as determined by a numerical weather predication model (COSMO-2) was compared to the in-situ measurements and accompanying remote sensing measurements from Kleine Scheidegg (below at 2060 m asl and in direct vicinity of JFJ) in Ketterer *et al.* (2014) and a clear underestimation of the PBL height for most of the cases was found.

CONCLUSIONS AND PERSPECTIVES

Despite the profound level of knowledge gained throughout the last decades, there are still important open questions with respect to the overall goal of the aerosol research performed at the JFJ, i.e. a better understanding of aerosols on climate.

On the one hand, the previous decades showed that long-term monitoring involves large efforts on all ends (from finances to manpower) to guarantee a data set that qualifies as a reliable input to statistics and models. As an example, the increased local emissions associated with the touristic activities at the JFJ have triggered further monitoring activities on the Jungfrau East Ridge (3700 m asl), a currently publicly inaccessible ridge 1.2 km distant from the JFJ site but with similar site characteristics. These additional measurements, using identical instruments at both sites, have started in 2014 and will be used to quantitatively assess the influence of the touristic activities.

A further example is the increasing number of break points in the data series with increasing length of the time series, as the monitoring technology advances and new instrumentation is introduced to replace older instrument types. The proper handling of such break points is and will be increasingly demanding (see e.g. previous trend analyses by Collaud Coen *et al.*, 2013 and Asmi *et al.*, 2013).

Compared to gas phase parameters performed at this and other sites, the two decades of extended aerosol measurements appear still rather short. To get the understanding of aerosol background trends onto a similar level of understanding as for the gas phase, it is necessary to

continue the aerosol monitoring on a long-term timescale. Only on a multi-decadal level the time series will be optimally beneficial for climate prediction.

Regarding the process mechanisms involved in aerosol-cloud interactions, much more research and fieldwork will be needed especially to investigate the exact role of the JFJ aerosol in the formation of mixed-phase clouds. Also for aerosol-cloud interactions, the real benefit for climate prediction will only pay off if the findings from real measurements have reached a statistically significant level. It is, therefore, important that the numerous advanced ice nuclei characterization techniques that have emerged in the last years will be applied for further investigations at the JFJ. A further important step forward would be to link measurements of cloud microphysical properties to radiation measurements in the cloud, preferably at several altitudes. However, due to the complex topography in the JFJ region this is not a simple task.

ACKNOWLEDGMENTS

A list of all scientists, technicians, administrators and other specialists that have shared their effort and passion to shed light on the Jungfraujoch aerosol would fill dozens of pages. Therefore, the authors would like to send big collective thanks to all involved researchers and their institutions. Special thanks go to the International Foundation High Altitude Research Stations Jungfraujoch and Gornergrat (HFSJG) for the opportunity to perform experiments on the

759 Jungfraujoch and for the continuous support by their custodians throughout the years. Also, the
760 aerosol research at the Jungfraujoch would not have been possible without a large number of
761 institutions providing financial support, as it is reflected in the comprehensive Acknowledgement
762 sections of the individual studies discussed in this review. These include MeteoSwiss through
763 their long-term financial support (since 1995) within the Swiss component of the Global
764 Atmosphere Watch Programme of the World Meteorological Organization, the Swiss Federal
765 Office for the Environment as part of the Swiss Air Quality Network (NABEL), the Swiss
766 National Science Foundation (SNSF), the UK Natural Environment Research Council (NERC),
767 the German Research Foundation (DFG), as well as the European Commission with a variety of
768 projects within FP5, FP6 and FP7, where within the latter the Infrastructure projects CREATE,
769 EUSAAR, and ACTRIS deserve special mentioning.

770

771

772

773

774

775 **REFERENCES**

776

777 Adams, F. C., Vancraen, M. J. and Vanespen, P. J. (1980). Enrichment of trace elements in
778 remote aerosols. *Env. Sci. Technol.* 14(8): 1002-1005. doi: 10.1021/es60168a007.
779 Alfarra, M. R., Paulsen, D., Gysel, M., Garforth, A. A., Dommen, J., Prévôt, A. S. H., Worsnop,
780 D. R., Baltensperger, U. and Coe, H. (2006). A mass spectrometric study of secondary
781 organic aerosols formed from the photooxidation of anthropogenic and biogenic
782 precursors in a reaction chamber. *Atmos. Chem. Phys.* 6(12): 5279-5293. doi:
783 10.5194/acp-6-5279-2006.
784 Andrews, E., Ogren, J. A., Bonasoni, P., Marinoni, A., Cuevas, E., Rodriguez, S., Sun, J. Y.,
785 Jaffe, D. A., Fischer, E. V., Baltensperger, U., Weingartner, E., Collaud Coen, M.,
786 Sharma, S., Macdonald, A. M., Leaitch, W. R., Lin, N. H., Laj, P., Arsov, T., Kalapov, I.,
787 Jefferson, A. and Sheridan, P. (2011). Climatology of aerosol radiative properties in the
788 free troposphere. *Atmos. Res.* 102(4): 365-393. doi: 10.1016/j.atmosres.2011.08.017.
789 Asmi, A., Wiedensohler, A., Laj, P., Fjaeraa, A. M., Sellegri, K., Birmili, W., Weingartner, E.,
790 Baltensperger, U., Zdimal, V., Zikova, N., Putaud, J. P., Marinoni, A., Tunved, P.,
791 Hansson, H. C., Fiebig, M., Kivekas, N., Lihavainen, H., Asmi, E., Ulevicius, V., Aalto,
792 P. P., Swietlicki, E., Kristensson, A., Mihalopoulos, N., Kalivitis, N., Kalapov, I., Kiss,
793 G., de Leeuw, G., Henzing, B., Harrison, R. M., Beddows, D., O'Dowd, C., Jennings, S.
794 G., Flentje, H., Weinhold, K., Meinhardt, F., Ries, L. and Kulmala, M. (2011). Number

795 size distributions and seasonality of submicron particles in Europe 2008-2009. *Atmos.*
796 *Chem. Phys.* 11(11): 5505-5538. doi: 10.5194/acp-11-5505-2011.
797 Asmi, A., Collaud Coen, M., Ogren, J. A., Andrews, E., Sheridan, P., Jefferson, A., Weingartner,
798 E., Baltensperger, U., Bukowiecki, N., Lihavainen, H., Kivekas, N., Asmi, E., Aalto, P.
799 P., Kulmala, M., Wiedensohler, A., Birmili, W., Hamed, A., O'Dowd, C., Jennings, S. G.,
800 Weller, R., Flentje, H., Fjaeraa, A. M., Fiebig, M., Myhre, C. L., Hallar, A. G., Swietlicki,
801 E., Kristensson, A. and Laj, P. (2013). Aerosol decadal trends - Part 2: In-situ aerosol
802 particle number concentrations at GAW and ACTRIS stations. *Atmos. Chem. Phys.* 13(2):
803 895-916. doi: 10.5194/acp-13-895-2013.
804 Baltensperger, U., Gäggeler, H. W., Jost, D. T., Emmenegger, M. and Naegeli, W. (1991).
805 Continuous background aerosol monitoring with the epiphaniometer. *Atmos. Environ.*
806 25(3-4): 629-634. doi: 10.1016/0960-1686(91)90060-k.
807 Baltensperger, U., Gäggeler, H. W., Jost, D. T., Lugauer, M., Schwikowski, M., Weingartner, E.
808 and Seibert, P. (1997). Aerosol climatology at the high-alpine site Jungfraujoch,
809 Switzerland. *J. Geophys. Res.* 102(D16): 19707-19715. doi: 10.1029/97jd00928.
810 Baltensperger, U., Schwikowski, M., Jost, D. T., Nyeki, S., Gäggeler, H. W. and Poulida, O.
811 (1998). Scavenging of atmospheric constituents in mixed phase clouds at the high-alpine

site Jungfraujoch part I: Basic concept and aerosol scavenging by clouds. *Atmos. Environ.* 32(23): 3975-3983. doi: 10.1016/s1352-2310(98)00051-x.

Baltensperger, U. (2010). Aerosols in Clearer Focus. *Science* 329(5998): 1474-1475. doi: 10.1126/science.1192930.

Balzani Lööv, J. M., Henne, S., Legreid, G., Staehelin, J., Reimann, S., Prévôt, A. S. H., Steinbacher, M. and Vollmer, M. K. (2008). Estimation of background concentrations of trace gases at the Swiss Alpine site Jungfraujoch (3580 m asl). *J. Geophys. Res.* 113. doi: 10.1029/2007jd009751.

Beddows, D. C. S., Dall'Osto, M., Harrison, R. M., Kulmala, M., Asmi, A., Wiedensohler, A., Laj, P., Fjaeraa, A. M., Sellegri, K., Birmili, W., Bukowiecki, N., Weingartner, E., Baltensperger, U., Zdimal, V., Zikova, N., Putaud, J. P., Marinoni, A., Tunved, P., Hansson, H. C., Fiebig, M., Kivekas, N., Swietlicki, E., Lihavainen, H., Asmi, E., Ulevicius, V., Aalto, P. P., Mihalopoulos, N., Kalivitis, N., Kalapov, I., Kiss, G., de Leeuw, G., Henzing, B., O'Dowd, C., Jennings, S. G., Flentje, H., Meinhardt, F., Ries, L., van der Gon, H. A. C. D. and Visschedijk, A. J. H. (2014). Variations in tropospheric submicron particle size distributions across the European continent 2008-2009. *Atmos. Chem. Phys.* 14(8): 4327-4348. doi: 10.5194/acp-14-4327-2014.

829 Boulon, J., Sellegri, K., Venzac, H., Picard, D., Weingartner, E., Wehrle, G., Collaud Coen, M.,
830 Buetikofer, R., Flueckiger, E., Baltensperger, U. and Laj, P. (2010). New particle
831 formation and ultrafine charged aerosol climatology at a high altitude site in the Alps
832 (Jungfraujoch, 3580 m a.s.l., Switzerland). *Atmos. Chem. Phys.* 10(19): 9333-9349. doi:
833 10.5194/acp-10-9333-2010.
834 Bukowiecki, N., Zieger, P., Weingartner, E., Jurányi, Z., Gysel, M., Neininger, B., Schneider, B.,
835 Hueglin, C., Ulrich, A., Wichser, A., Henne, S., Brunner, D., Kaegi, R., Schwikowski, M.,
836 Tobler, L., Wienhold, F. G., Engel, I., Buchmann, B., Peter, T. and Baltensperger, U.
837 (2011). Ground-based and airborne in-situ measurements of the Eyjafjallajokull volcanic
838 aerosol plume in Switzerland in spring 2010. *Atmos. Chem. Phys.* 11(19): 10011-10030.
839 doi: 10.5194/acp-11-10011-2011.
840 Bundke, U., Nillius, B., Jaenicke, R., Wetter, T., Klein, H. and Bingemer, H. (2008). The fast Ice
841 Nucleus chamber FINCH. *Atmos. Res.* 90(2-4): 180-186. doi:
842 10.1016/j.atmosres.2008.02.008.
843 Burtscher, H., Baltensperger, U., Bukowiecki, N., Cohn, P., Huglin, C., Mohr, M., Matter, U.,
844 Nyeki, S., Schmatloch, V., Streit, N. and Weingartner, E. (2001). Separation of volatile
845 and non-volatile aerosol fractions by thermodesorption: instrumental development and
846 applications. *J. Aerosol Sci.* 32(4): 427-442. doi: 10.1016/s0021-8502(00)00089-6.

847 Cavalli, F., Viana, M., Yttri, K. E., Genberg, J. and Putaud, J. P. (2010). Toward a standardised
848 thermal-optical protocol for measuring atmospheric organic and elemental carbon: the
849 EUSAAR protocol. *Atmos. Meas. Tech.* 3(1): 79-89. doi: 10.5194/amt-3-79-2010.
850 Chou, C., Stetzer, O., Weingartner, E., Jurányi, Z., Kanji, Z. A. and Lohmann, U. (2011). Ice
851 nuclei properties within a Saharan dust event at the Jungfraujoch in the Swiss Alps.
852 *Atmos. Chem. Phys.* 11(10): 4725-4738. doi: 10.5194/acp-11-4725-2011.
853 Choularton, T. W., Bower, K. N., Weingartner, E., Crawford, I., Coe, H., Gallagher, M. W.,
854 Flynn, M., Crosier, J., Connolly, P., Targino, A., Alfarra, M. R., Baltensperger, U.,
855 Sjogren, S., Verheggen, B., Cozic, J. and Gysel, M. (2008). The influence of small aerosol
856 particles on the properties of water and ice clouds. *Farad. Discuss.* 137: 205-222. doi:
857 10.1039/b702722m.
858 Collaud Coen, M., Weingartner, E., Schaub, D., Hueglin, C., Corrigan, C., Henning, S.,
859 Schwikowski, M. and Baltensperger, U. (2004). Saharan dust events at the Jungfraujoch:
860 detection by wavelength dependence of the single scattering albedo and first climatology
861 analysis. *Atmos. Chem. Phys.* 4: 2465-2480.
862 Collaud Coen, M., Weingartner, E., Nyeki, S., Cozic, J., Henning, S., Verheggen, B., Gehrig, R.
863 and Baltensperger, U. (2007). Long-term trend analysis of aerosol variables at the high-
864 alpine site Jungfraujoch. *J. Geophys. Res.* 112(D13). doi: 10.1029/2006jd007995.

865 Collaud Coen, M., Weingartner, E., Apituley, A., Ceburnis, D., Fierz-Schmidhauser, R., Flentje,
866 H., Henzing, J. S., Jennings, S. G., Moerman, M., Petzold, A., Schmid, O. and
867 Baltensperger, U. (2010). Minimizing light absorption measurement artifacts of the
868 Aethalometer: evaluation of five correction algorithms. *Atmos. Meas. Tech.* 3(2): 457-
869 474.

870 Collaud Coen, M., Weingartner, E., Furger, M., Nyeki, S., Prévôt, A. S. H., Steinbacher, M. and
871 Baltensperger, U. (2011). Aerosol climatology and planetary boundary influence at the
872 Jungfraujoch analyzed by synoptic weather types. *Atmos. Chem. Phys.* 11(12): 5931-
873 5944. doi: 10.5194/acp-11-5931-2011.

874 Collaud Coen, M., Andrews, E., Asmi, A., Baltensperger, U., Bukowiecki, N., Day, D., Fiebig,
875 M., Fjaeraa, A. M., Flentje, H., Hyvarinen, A., Jefferson, A., Jennings, S. G., Kouvarakis,
876 G., Lihavainen, H., Myhre, C. L., Malm, W. C., Mihapopoulos, N., Molenar, J. V.,
877 O'Dowd, C., Ogren, J. A., Schichtel, B. A., Sheridan, P., Virkkula, A., Weingartner, E.,
878 Weller, R. and Laj, P. (2013). Aerosol decadal trends - Part 1: In-situ optical
879 measurements at GAW and IMPROVE stations. *Atmos. Chem. Phys.* 13(2): 869-894. doi:
880 10.5194/acp-13-869-2013.

881 Conen, F., Rodriguez, S., Hueglin, C., Henne, S., Herrmann, E., Bukowiecki, N. and Alewell, C.
882 (2015). Atmospheric ice nuclei at the high-altitude observatory Jungfraujoch, Switzerland.
883 *Tellus Ser. B* 67. doi: 10.3402/tellusb.v67.25014.
884 Cozic, J., Verheggen, B., Mertes, S., Connolly, P., Bower, K., Petzold, A., Baltensperger, U. and
885 Weingartner, E. (2007). Scavenging of black carbon in mixed phase clouds at the high
886 alpine site Jungfraujoch. *Atmos. Chem. Phys.* 7(7): 1797-1807.
887 Cozic, J., Verheggen, B., Weingartner, E., Crosier, J., Bower, K. N., Flynn, M., Coe, H.,
888 Henning, S., Steinbacher, M., Henne, S., Collaud Coen, M., Petzold, A. and
889 Baltensperger, U. (2008a). Chemical composition of free tropospheric aerosol for PM1
890 and coarse mode at the high alpine site Jungfraujoch. *Atmos. Chem. Phys.* 8(2): 407-423.
891 Cozic, J., Mertes, S., Verheggen, B., Cziczo, D. J., Gallavardin, S. J., Walter, S., Baltensperger,
892 U. and Weingartner, E. (2008b). Black carbon enrichment in atmospheric ice particle
893 residuals observed in lower tropospheric mixed phase clouds. *J. Geophys. Res.* 113(D15).
894 doi: 10.1029/2007jd009266.
895 Cziczo, D. J., Stetzer, O., Worringen, A., Ebert, M., Weinbruch, S., Kamphus, M., Gallavardin,
896 S. J., Curtius, J., Borrmann, S., Froyd, K. D., Mertes, S., Moehler, O. and Lohmann, U.
897 (2009). Inadvertent climate modification due to anthropogenic lead. *Nat. Geosci.* 2(5):
898 333-336. doi: 10.1038/ngeo499.

899 Dams, R. and Dejonge, J. (1976). Chemical composition of Swiss aerosols from Jungfraujoch.
900 *Atmos. Env.* 10(12): 1079-1084. doi: 10.1016/0004-6981(76)90117-7.
901 Duplissy, J., DeCarlo, P. F., Dommen, J., Alfarra, M. R., Metzger, A., Barmpadimos, I., Prévôt,
902 A. S. H., Weingartner, E., Tritscher, T., Gysel, M., Aiken, A. C., Jimenez, J. L.,
903 Canagaratna, M. R., Worsnop, D. R., Collins, D. R., Tomlinson, J. and Baltensperger, U.
904 (2011). Relating hygroscopicity and composition of organic aerosol particulate matter.
905 *Atmos. Chem. Phys.* 11(3): 1155-1165. doi: 10.5194/acp-11-1155-2011.
906 Ebert, M., Worringen, A., Benker, N., Mertes, S., Weingartner, E. and Weinbruch, S. (2011).
907 Chemical composition and mixing-state of ice residuals sampled within mixed phase
908 clouds. *Atmos. Chem. Phys.* 11(6): 2805-2816. doi: 10.5194/acp-11-2805-2011.
909 Ehrman, S. H., Schwikowski, M., Baltensperger, U. and Gäggeler, H. W. (2001). Sampling and
910 chemical analysis of ice crystals as a function of size. *Atmos. Env.* 35(31): 5371-5376.
911 doi: 10.1016/s1352-2310(01)00294-1.
912 Fierz-Schmidhauser, R., Zieger, P., Gysel, M., Kammermann, L., DeCarlo, P. F., Baltensperger,
913 U. and Weingartner, E. (2010a). Measured and predicted aerosol light scattering
914 enhancement factors at the high alpine site Jungfraujoch. *Atmos. Chem. Phys.* 10(5):
915 2319-2333.

916 Fierz-Schmidhauser, R., Zieger, P., Wehrle, G., Jefferson, A., Ogren, J. A., Baltensperger, U. and
917 Weingartner, E. (2010b). Measurement of relative humidity dependent light scattering of
918 aerosols. *Atmos. Meas. Tech.* 3(1): 39-50.
919 Fröhlich, R., Cubison, M. J., Slowik, J. G., Bukowiecki, N., Prévôt, A. S. H., Baltensperger, U.,
920 Schneider, J., Kimmel, J. R., Gonin, M., Rohner, U., Worsnop, D. R. and Jayne, J. T.
921 (2013). The ToF-ACSM: a portable aerosol chemical speciation monitor with TOFMS
922 detection. *Atmos. Meas. Tech.* 6(11): 3225-3241. doi: 10.5194/amt-6-3225-2013.
923 Fröhlich, R., Cubison, M. J., Slowik, J. G., Bukowiecki, N., Canonaco, F., Henne, S., Herrmann,
924 E., Gysel, M., Steinbacher, M., Baltensperger, U. and Prévôt, A. S. H. (2015). Fourteen
925 months of on-line measurements of the non-refractory submicron aerosol at the
926 Jungfraujoch (3580 m a.s.l.) – chemical composition, origins and organic aerosol sources.
927 *Atmos. Chem. Phys. Discuss*. 15: 18225-18284. doi:10.5194/acpd-15-18225-2015. .
928 Gäggeler, H. W., Baltensperger, U., Emmenegger, M., Jost, D. T., Schmidt Ott, A., Haller, P. and
929 Hofmann, M. (1989). The epiphaniometer, a new device for continuous aerosol
930 monitoring. *J. Aerosol Sci.* 20(5): 557-564. doi: 10.1016/0021-8502(89)90101-8.
931 Gehrig, R. (1986). National observation network for air pollutants (NABEL) - present data -
932 planned extensions. *Sozial- und Praventivmedizin* 31(1): 46-48. doi: 10.1007/bf02103749.

933 Griffiths, A. D., Conen, F., Weingartner, E., Zimmermann, L., Chambers, S. D., Williams, A. G.
934 and Steinbacher, M. (2014). Surface-to-mountaintop transport characterised by radon
935 observations at the Jungfraujoch. *Atmos. Chem. Phys.* 14(23): 12763-12779. doi:
936 10.5194/acp-14-12763-2014.
937 Grobety, B., Meier, M. and Neururer, C. (2011). Single particle analysis of aerosols from Saharan
938 dust events. Bern, Switzerland: International Foundation High Altitude Research Stations
939 Jungfraujoch + Gornergrat HFSJG, Retrieved from
940 http://hfsjg.ch/reports/2011/pdf/108_Meier_UniFR_f.pdf.
941 Hammer, E., Bukowiecki, N., Gysel, M., Jurányi, Z., Hoyle, C. R., Vogt, R., Baltensperger, U.
942 and Weingartner, E. (2014a). Investigation of the effective peak supersaturation for
943 liquid-phase clouds at the high-alpine site Jungfraujoch, Switzerland (3580 m a.s.l.).
944 *Atmos. Chem. Phys.* 14(2): 1123-1139. doi: 10.5194/acp-14-1123-2014.
945 Hammer, E., Bukowiecki, N., Luo, B. P., Lohmann, U., Marcolli, C., Weingartner, E.,
946 Baltensperger, U. and Hoyle, C. R. (2014b). Sensitivity estimations for cloud droplet
947 formation in the vicinity of the high alpine research station Jungfraujoch (3580 m a.s.l.).
948 *Atmos. Chem. Phys. Discuss.* 14(19): 25967-26002. doi: 10.5194/acpd-14-25967-2014.

949 Henne, S., Brunner, D., Folini, D., Solberg, S., Klausen, J. and Buchmann, B. (2010). Assessment
950 of parameters describing representativeness of air quality in-situ measurement sites.
951 *Atmos. Chem. Phys.* 10(8): 3561-3581. doi: 10.5194/acp-10-3561-2010.
952 Henneberger, J., Fugal, J. P., Stetzer, O. and Lohmann, U. (2013). HOLIMO II: a digital
953 holographic instrument for ground-based in situ observations of microphysical properties
954 of mixed-phase clouds. *Atmos. Meas. Tech.* 6(11): 2975-2987. doi: 10.5194/amt-6-2975-
955 2013.
956 Henning, S., Weingartner, E., Schmidt, S., Wendisch, M., Gäggeler, H. W. and Baltensperger, U.
957 (2002). Size-dependent aerosol activation at the high-alpine site Jungfraujoch (3580 m
958 asl). *Tellus Ser. B* 54(1): 82-95. doi: 10.1034/j.1600-0889.2002.00299.x.
959 Henning, S., Weingartner, E., Schwikowski, M., Gäggeler, H. W., Gehrig, R., Hinz, K. P.,
960 Trimborn, A., Spengler, B. and Baltensperger, U. (2003). Seasonal variation of water-
961 soluble ions of the aerosol at the high-alpine site Jungfraujoch (3580 m asl). *J. Geophys.*
962 *Res.* 108(D1). doi: 10.1029/2002jd002439.
963 Henning, S., Bojinski, S., Diehl, K., Ghan, S., Nyeki, S., Weingartner, E., Wurzler, S. and
964 Baltensperger, U. (2004). Aerosol partitioning in natural mixed-phase clouds. *Geophys.*
965 *Res. Lett.* 31(6). doi: 10.1029/2003gl019025.

966 Herrmann, E., Weingartner, E., Henne, S., Vuilleumier, L., Bukowiecki, N., Steinbacher, M.,
967 Conen, F., Collaud Coen, M., Hammer, E., Jurányi, Z., Baltensperger, U. and Gysel, M.
968 (2015). Analysis of long-term aerosol size distribution data from Jungfraujoch with
969 emphasis on free tropospheric conditions, cloud influence, and air mass transport. *J.*
970 *Geophys. Res.* submitted.
971 Hoose, C., Lohmann, U., Stier, P., Verheggen, B. and Weingartner, E. (2008). Aerosol processing
972 in mixed-phase clouds in ECHAM5-HAM: Model description and comparison to
973 observations. *J. Geophys. Res.* 113(D7). doi: 10.1029/2007jd009251.
974 Hoppel, W. A., Frick, G. M. and Larson, R. E. (1986). Effect of nonprecipitating clouds on the
975 aerosol size distribution in the marine boundary layer. *Geophys. Res. Lett.* 13(2): 125-128.
976 doi: 10.1029/GL013i002p00125.
977 Hoyle, C. R., Webster, C. S., Rieder, H. E., Hammer, E., Gysel, M., Bukowiecki, N.,
978 Weingartner, E., Steinbacher, M. and Baltensperger, U. (2015). Chemical and physical
979 influences on aerosol activation in liquid clouds: An empirical study based on
980 observations from the Jungfraujoch, Switzerland. *Atmos. Chem. Phys. Discuss.* 15: 15469-
981 15510. doi:10.5194/acpd-15-15469-2015.

Ingold, T., Matzler, C., Kampfer, N. and Heimo, A. (2001). Aerosol optical depth measurements by means of a Sun photometer network in Switzerland. *J. Geophys. Res.* 106(D21): 27537-27554. doi: 10.1029/2000jd000088.

Jimenez, J. L., Canagaratna, M. R., Donahue, N. M., Prévôt, A. S. H., Zhang, Q., Kroll, J. H., DeCarlo, P. F., Allan, J. D., Coe, H., Ng, N. L., Aiken, A. C., Docherty, K. S., Ulbrich, I. M., Grieshop, A. P., Robinson, A. L., Duplissy, J., Smith, J. D., Wilson, K. R., Lanz, V. A., Hueglin, C., Sun, Y. L., Tian, J., Laaksonen, A., Raatikainen, T., Rautiainen, J., Vaattovaara, P., Ehn, M., Kulmala, M., Tomlinson, J. M., Collins, D. R., Cubison, M. J., Dunlea, E. J., Huffman, J. A., Onasch, T. B., Alfarra, M. R., Williams, P. I., Bower, K., Kondo, Y., Schneider, J., Drewnick, F., Borrmann, S., Weimer, S., Demerjian, K., Salcedo, D., Cottrell, L., Griffin, R., Takami, A., Miyoshi, T., Hatakeyama, S., Shimono, A., Sun, J. Y., Zhang, Y. M., Dzepina, K., Kimmel, J. R., Sueper, D., Jayne, J. T., Herndon, S. C., Trimborn, A. M., Williams, L. R., Wood, E. C., Middlebrook, A. M., Kolb, C. E., Baltensperger, U. and Worsnop, D. R. (2009). Evolution of organic aerosols in the atmosphere. *Science* 326(5959): 1525-1529. doi: 10.1126/science.1180353.

Jurányi, Z., Gysel, M., Weingartner, E., DeCarlo, P. F., Kammermann, L. and Baltensperger, U. (2010). Measured and modelled cloud condensation nuclei number concentration at the

high alpine site Jungfraujoch. *Atmos. Chem. Phys.* 10(16): 7891-7906. doi: 10.5194/acp-10-7891-2010.

Jurányi, Z., Gysel, M., Weingartner, E., Bukowiecki, N., Kammermann, L. and Baltensperger, U. (2011). A 17 month climatology of the cloud condensation nuclei number concentration at the high alpine site Jungfraujoch. *J. Geophys. Res.* 116. doi: 10.1029/2010jd015199.

Kammermann, L., Gysel, M., Weingartner, E. and Baltensperger, U. (2010). 13-month climatology of the aerosol hygroscopicity at the free tropospheric site Jungfraujoch (3580 m a.s.l.). *Atmos. Chem. Phys.* 10(22): 10717-10732. doi: 10.5194/acp-10-10717-2010.

Kamphus, M., Ettner-Mahl, M., Klimach, T., Drewnick, F., Keller, L., Cziczo, D. J., Mertes, S., Borrmann, S. and Curtius, J. (2010). Chemical composition of ambient aerosol, ice residues and cloud droplet residues in mixed-phase clouds: single particle analysis during the Cloud and Aerosol Characterization Experiment (CLACE 6). *Atmos. Chem. Phys.* 10(16): 8077-8095. doi: 10.5194/acp-10-8077-2010.

Kanji, Z. A., Henneberger, J., Boose, Y. and Lacher, L. (2014). Field measurements of aerosols acting as ice nucleating particles and their influence on mixed-phase clouds. Bern, Switzerland: International Foundation High Altitude Research Stations Jungfraujoch + Gornergrat HFSJG, Retrieved from http://hfsjg.ch/reports/2014/pdf/110_ETHZ_Kanji_cf.pdf.

1017 Ketterer, C., Zieger, P., Bukowiecki, N., Collaud Coen, M., Maier, O., Ruffieux, D. and
1018 Weingartner, E. (2014). Investigation of the planetary boundary layer in the Swiss Alps
1019 using remote sensing and in situ measurements. *Bound.-Layer Meteor.* 151(2): 317-334.
1020 doi: 10.1007/s10546-013-9897-8.
1021 Kristiansen, N. I., Stohl, A., Prata, A. J., Bukowiecki, N., Dacre, H., Eckhardt, S., Henne, S.,
1022 Hort, M. C., Johnson, B. T., Marenco, F., Neininger, B., Reitebuch, O., Seibert, P.,
1023 Thomson, D. J., Webster, H. N. and Weinzierl, B. (2012). Performance assessment of a
1024 volcanic ash transport model mini-ensemble used for inverse modeling of the 2010
1025 Eyjafjallajokull eruption. *J. Geophys. Res.* 117. doi: 10.1029/2011jd016844.
1026 Krivacsy, Z., Gelencser, A., Kiss, G., Meszaros, E., Molnar, A., Hoffer, A., Meszaros, T.,
1027 Sarvari, Z., Temesi, D., Varga, B., Baltensperger, U., Nyeki, S. and Weingartner, E.
1028 (2001). Study on the chemical character of water soluble organic compounds in fine
1029 atmospheric aerosol at the Jungfraujoch. *J. Atmos. Chem.* 39(3): 235-259. doi:
1030 10.1023/a:1010637003083.
1031 Kupiszewski, P., Weingartner, E., Vochezer, P., Schnaiter, M., Bigi, A., Gysel, M., Rosati, B.,
1032 Toprak, E., Mertes, S., and Baltensperger, U. (2015). The Ice Selective Inlet: a novel
1033 technique for exclusive extraction of pristine ice crystals in mixed-phase clouds. *Atmos.*
1034 *Meas. Tech.* 8: 3087-3106. doi:10.5194/amt-8-3087-2015.

1035 Lanz, V. A., Prévôt, A. S. H., Alfarra, M. R., Weimer, S., Mohr, C., DeCarlo, P. F., Gianini, M.
1036 F. D., Hueglin, C., Schneider, J., Favez, O., D'Anna, B., George, C. and Baltensperger, U.
1037 (2010). Characterization of aerosol chemical composition with aerosol mass spectrometry
1038 in Central Europe: an overview. *Atmos. Chem. Phys.* 10(21): 10453-10471. doi:
1039 10.5194/acp-10-10453-2010.
1040 Lavanchy, V. M. H., Gäggeler, H. W., Nyeki, S. and Baltensperger, U. (1999). Elemental carbon
1041 (EC) and black carbon (BC) measurements with a thermal method and an aethalometer at
1042 the high-alpine research station Jungfraujoch. *Atmos. Env.* 33(17): 2759-2769. doi:
1043 10.1016/s1352-2310(98)00328-8.
1044 Liu, D., Flynn, M., Gysel, M., Targino, A., Crawford, I., Bower, K., Choularton, T., Jurányi, Z.,
1045 Steinbacher, M., Hueglin, C., Curtius, J., Kampus, M., Petzold, A., Weingartner, E.,
1046 Baltensperger, U. and Coe, H. (2010). Single particle characterization of black carbon
1047 aerosols at a tropospheric alpine site in Switzerland. *Atmos. Chem. Phys.* 10(15): 7389-
1048 7407. doi: 10.5194/acp-10-7389-2010.
1049 Lohmann, U. and Diehl, K. (2006). Sensitivity studies of the importance of dust ice nuclei for the
1050 indirect aerosol effect on stratiform mixed-phase clouds. *J. Atmos. Sci.* 63(3): 968-982.
1051 doi: 10.1175/jas3662.1.

1052 Lugauer, M., Baltensperger, U., Furger, M., Gäggeler, H. W., Jost, D. T., Schwikowski, M. and
1053 Wanner, H. (1998). Aerosol transport to the high Alpine sites Jungfraujoch (3454 m asl)
1054 and Colle Gnifetti (4452 m asl). *Tellus Ser. B* 50(1): 76-92. doi: 10.1034/j.1600-
1055 0889.1998.00006.x.
1056 Lugauer, M., Baltensperger, U., Furger, M., Gäggeler, H. W., Jost, D. T., Nyeki, S. and
1057 Schwikowski, M. (2000). Influences of vertical transport and scavenging on aerosol
1058 particle surface area and radon decay product concentrations at the Jungfraujoch (3454 m
1059 above sea level). *J. Geophys. Res.* 105(D15): 19869-19879. doi: 10.1029/2000jd900184.
1060 Mann, G. W., Carslaw, K. S., Reddington, C. L., Pringle, K. J., Schulz, M., Asmi, A., Spracklen,
1061 D. V., Ridley, D. A., Woodhouse, M. T., Lee, L. A., Zhang, K., Ghan, S. J., Easter, R. C.,
1062 Liu, X., Stier, P., Lee, Y. H., Adams, P. J., Tost, H., Lelieveld, J., Bauer, S. E., Tsigaridis,
1063 K., van Noije, T. P. C., Strunk, A., Vignati, E., Bellouin, N., Dalvi, M., Johnson, C. E.,
1064 Bergman, T., Kokkola, H., von Salzen, K., Yu, F., Luo, G., Petzold, A., Heintzenberg, J.,
1065 Clarke, A., Ogren, A., Gras, J., Baltensperger, U., Kaminski, U., Jennings, S. G., O'Dowd,
1066 C. D., Harrison, R. M., Beddows, D. C. S., Kulmala, M., Viisanen, Y., Ulevicius, V.,
1067 Mihalopoulos, N., Zdimal, V., Fiebig, M., Hansson, H. C., Swietlicki, E. and Henzing, J.
1068 S. (2014). Intercomparison and evaluation of global aerosol microphysical properties

among AeroCom models of a range of complexity. *Atmos. Chem. Phys.* 14(9): 4679-4713. doi: 10.5194/acp-14-4679-2014.

Manninen, H. E., Nieminen, T., Asmi, E., Gagne, S., Hakkinen, S., Lehtipalo, K., Aalto, P., Vana, M., Mirme, A., Mirme, S., Horrak, U., Plass-Duelmer, C., Stange, G., Kiss, G., Hoffer, A., Toeroe, N., Moerman, M., Henzing, B., de Leeuw, G., Brinkenberg, M., Kouvarakis, G. N., Bougiatioti, A., Mihalopoulos, N., O'Dowd, C., Ceburnis, D., Arneth, A., Svenningsson, B., Swietlicki, E., Tarozzi, L., Decesari, S., Facchini, M. C., Birmili, W., Sonntag, A., Wiedensohler, A., Boulon, J., Sellegri, K., Laj, P., Gysel, M., Bukowiecki, N., Weingartner, E., Wehrle, G., Laaksonen, A., Hamed, A., Joutsensaari, J., Petaja, T., Kerminen, V. M. and Kulmala, M. (2010). EUCAARI ion spectrometer measurements at 12 European sites - analysis of new particle formation events. *Atmos. Chem. Phys.* 10(16): 7907-7927. doi: 10.5194/acp-10-7907-2010.

McFiggans, G., Artaxo, P., Baltensperger, U., Coe, H., Facchini, M. C., Feingold, G., Fuzzi, S., Gysel, M., Laaksonen, A., Lohmann, U., Mentel, T. F., Murphy, D. M., O'Dowd, C. D., Snider, J. R. and Weingartner, E. (2006). The effect of physical and chemical aerosol properties on warm cloud droplet activation. *Atmos. Chem. Phys.* 6(9): 2593-2649. doi: 10.5194/acp-6-2593-2006.

1086 Mertes, S., Verheggen, B., Walter, S., Connolly, P., Ebert, M., Schneider, J., Bower, K. N.,
1087 Cozic, J., Weinbruch, S., Baltensperger, U. and Weingartner, E. (2007). Counterflow
1088 virtual impact or based collection of small ice particles in mixed-phase clouds for the
1089 physico-chemical characterization of tropospheric ice nuclei : Sampler description and
1090 first case study. *Aerosol Sci. Technol.* 41(9): 848-864. doi: 10.1080/02786820701501881.
1091 Morrical, B. D. and Zenobi, R. (2002). Detection of polycyclic aromatic compounds at
1092 Jungfraujoch high-alpine research station using two-step laser mass spectrometry. *Int. J.*
1093 *Environ. Anal. Chem.* 82(6): 377-385. doi: 10.1080/0306731021000003464.
1094 Muhlbauer, A. and Lohmann, U. (2008). Sensitivity studies of the role of aerosols in warm-phase
1095 orographic precipitation in different dynamical flow regimes. *J. Atmos. Sci.* 65(8): 2522-
1096 2542. doi: 10.1175/2007jas2492.1.
1097 Nessler, R., Bukowiecki, N., Henning, S., Weingartner, E., Calpini, B. and Baltensperger, U.
1098 (2003). Simultaneous dry and ambient measurements of aerosol size distributions at the
1099 Jungfraujoch. *Tellus Ser. B* 55(3): 808-819. doi: 10.1034/j.1600-0889.2003.00067.x.
1100 Nessler, R., Weingartner, E. and Baltensperger, U. (2005a). Adaptation of dry nephelometer
1101 measurements to ambient conditions at the Jungfraujoch. *Environ. Sci. Technol.* 39(7):
1102 2219-2228. doi: 10.1021/es035450g.

1103 Nessler, R., Weingartner, E. and Baltensperger, U. (2005b). Effect of humidity on aerosol light
1104 absorption and its implications for extinction and the single scattering albedo illustrated
1105 for a site in the lower free troposphere. *J. Aerosol Sci.* 36(8): 958-972. doi:
1106 10.1016/j.jaerosci.2004.11.012.
1107 Nyeki, S., Baltensperger, U., Colbeck, I., Jost, D. T., Weingartner, E. and Gäggeler, H. W.
1108 (1998a). The Jungfraujoch high-Alpine research station (3454m) as a background clean
1109 continental site for the measurement of aerosol parameters. *J. Geophys. Res.* 103(D6):
1110 6097-6107. doi: 10.1029/97jd03123.
1111 Nyeki, S., Li, F., Weingartner, E., Streit, N., Colbeck, I., Gäggeler, H. W. and Baltensperger, U.
1112 (1998b). The background aerosol size distribution in the free troposphere: An analysis of
1113 the annual cycle at a high-alpine site. *J. Geophys. Res.* 103(D24): 31749-31761. doi:
1114 10.1029/1998jd200029.
1115 Nyeki, S., Kalberer, M., Lugauer, M., Weingartner, E., Petzold, A., Schroder, F., Colbeck, I. and
1116 Baltensperger, U. (1999). Condensation nuclei (CN) and ultrafine CN in the free
1117 troposphere to 12 km: A case study over the Jungfraujoch high-alpine research station.
1118 *Geophys. Res. Lett.* 26(14): 2195-2198. doi: 10.1029/1999gl900473.
1119 Nyeki, S., Kalberer, M., Colbeck, I., De Wekker, S., Furger, M., Gäggeler, H. W., Kossmann, M.,
1120 Lugauer, M., Steyn, D., Weingartner, E., Wirth, M. and Baltensperger, U. (2000).

Convective boundary layer evolution to 4 km asl over high-alpine terrain: Airborne lidar observations in the Alps. *Geophys. Res. Lett.* 27(5): 689-692. doi: 10.1029/1999gl010928.

Nyeki, S., Eleftheriadis, K., Baltensperger, U., Colbeck, I., Fiebig, M., Fix, A., Kiemle, C., Lazaridis, M. and Petzold, A. (2002). Airborne lidar and in-situ aerosol observations of an elevated layer, leeward of the European Alps and Apennines. *Geophys. Res. Lett.* 29(17). doi: 10.1029/2002gl014897.

Nyeki, S., Halios, C. H., Baum, W., Eleftheriadis, K., Flentje, H., Groebner, J., Vuilleumier, L. and Wehrli, C. (2012). Ground-based aerosol optical depth trends at three high-altitude sites in Switzerland and southern Germany from 1995 to 2010. *J. Geophys. Res.* 117. doi: 10.1029/2012jd017493.

Paramonov, M., Kerminen, V.-M., Gysel, M., Aalto, P. P., Andreae, M. O., Asmi, E., Baltensperger, U., Bougiatioti, A., Brus, D., Frank, D., Good, N., Gunthe, S., Hao, L., Irwin, M., Jaatinen, A., Jurányi, Z., King, S. M., Kortelainen, A., Kristensson, A., Lihavainen, H., Kulmala, M., Lohmann, U., Martin, S. T., McFiggans, G., Mihalopoulos, N., Nenes, A., O'Dowd, C. D., Ovadnevaite, J., Petäjä, T., Pöschl, U., Roberts, G. C., Rose, D., Svenningson, B., Swietlicki, E., Weingartner, E., Whitehead, J., Wiedensohler, A., Wittbom, C. and Sierau, B. (2015). A synthesis of cloud condensation nuclei counter

(CCNC) measurements within the EUCAARI network. *Atmos. Chem. Phys. Discuss.* 15: 15039-15086. doi:10.5194/acpd-15-15039-2015.

Petters, M. D. and Kreidenweis, S. M. (2007). A single parameter representation of hygroscopic growth and cloud condensation nucleus activity. *Atmos. Chem. Phys.* 7(8): 1961-1971.

Petzold, A., Weinzierl, B., Huntrieser, H., Stohl, A., Real, E., Cozic, J., Fiebig, M., Hendricks, J., Lauer, A., Law, K., Roiger, A., Schlager, H. and Weingartner, E. (2007). Perturbation of the European free troposphere aerosol by North American forest fire plumes during the ICARTT-ITOP experiment in summer 2004. *Atmos. Chem. Phys.* 7(19): 5105-5127.

Petzold, A., Ogren, J. A., Fiebig, M., Laj, P., Li, S. M., Baltensperger, U., Holzer-Popp, T., Kinne, S., Pappalardo, G., Sugimoto, N., Wehrli, C., Wiedensohler, A. and Zhang, X. Y. (2013). Recommendations for reporting "black carbon" measurements. *Atmos. Chem. Phys.* 13(16): 8365-8379. doi: 10.5194/acp-13-8365-2013.

Reddington, C. L., Carslaw, K. S., Spracklen, D. V., Frontoso, M. G., Collins, L., Merikanto, J., Minikin, A., Hamburger, T., Coe, H., Kulmala, M., Aalto, P., Flentje, H., Plass-Duelmer, C., Birmili, W., Wiedensohler, A., Wehner, B., Tuch, T., Sonntag, A., O'Dowd, C. D., Jennings, S. G., Dupuy, R., Baltensperger, U., Weingartner, E., Hansson, H. C., Tunved, P., Laj, P., Sellegri, K., Boulon, J., Putaud, J. P., Gruening, C., Swietlicki, E., Roldin, P., Henzing, J. S., Moerman, M., Mihalopoulos, N., Kouvarakis, G., Zdimal, V., Zikova, N.,

1156 Marinoni, A., Bonasoni, P. and Duchi, R. (2011). Primary versus secondary contributions
1157 to particle number concentrations in the European boundary layer. *Atmos. Chem. Phys.*
1158 11(23): 12007-12036. doi: 10.5194/acp-11-12007-2011.
1159 Schüepp, M. (1979). Witterungsklimatologie, Klimatologie der Schweiz, Band III, Beilage zu
1160 den Annalen 1978, (available from MeteoSwiss, Zürich, Switzerland).
1161 Schwikowski, M., Baltensperger, U., Gäggeler, H. W. and Poulida, O. (1998). Scavenging of
1162 atmospheric constituents in mixed phase clouds at the high-alpine site Jungfraujoch part
1163 III: Quantification of the removal of chemical species by precipitating snow. *Atmos. Env.*
1164 32(23): 4001-4010. doi: 10.1016/s1352-2310(98)00050-8.
1165 Sjogren, S., Gysel, M., Weingartner, E., Alfarra, M. R., Duplissy, J., Cozic, J., Crosier, J., Coe,
1166 H. and Baltensperger, U. (2008). Hygroscopicity of the submicrometer aerosol at the
1167 high-alpine site Jungfraujoch, 3580 m a.s.l., Switzerland. *Atmos. Chem. Phys.* 8(18):
1168 5715-5729.
1169 Spiegel, J. K., Zieger, P., Bukowiecki, N., Hammer, E., Weingartner, E. and Eugster, W. (2012).
1170 Evaluating the capabilities and uncertainties of droplet measurements for the fog droplet
1171 spectrometer (FM-100). *Atmos. Meas. Tech.* 5(9): 2237-2260. doi: 10.5194/amt-5-2237-
1172 2012.

1173 Spracklen, D. V., Carslaw, K. S., Merikanto, J., Mann, G. W., Reddington, C. L., Pickering, S.,
1174 Ogren, J. A., Andrews, E., Baltensperger, U., Weingartner, E., Boy, M., Kulmala, M.,
1175 Laakso, L., Lihavainen, H., Kivekas, N., Komppula, M., Mihalopoulos, N., Kouvarakis,
1176 G., Jennings, S. G., O'Dowd, C., Birmili, W., Wiedensohler, A., Weller, R., Gras, J., Laj,
1177 P., Sellegri, K., Bonn, B., Krejci, R., Laaksonen, A., Hamed, A., Minikin, A., Harrison, R.
1178 M., Talbot, R. and Sun, J. (2010). Explaining global surface aerosol number
1179 concentrations in terms of primary emissions and particle formation. *Atmos. Chem. Phys.*
1180 10(10): 4775-4793. doi: 10.5194/acp-10-4775-2010.
1181 Streit, N., Weingartner, E., Zellweger, C., Schwikowski, M., Gäggeler, H. W. and Baltensperger,
1182 U. (2000). Characterization of size-fractionated aerosol from the Jungfraujoch (3580 m
1183 asl) using total reflection X-ray fluorescence (TXRF). *Int. J. Environ. Anal. Chem.* 76(1):
1184 1-16. doi: 10.1080/03067310008034114.
1185 Sturm, P., Tuzson, B., Henne, S. and Emmenegger, L. (2013). Tracking isotopic signatures of
1186 CO2 at the high altitude site Jungfraujoch with laser spectroscopy: analytical
1187 improvements and representative results. *Atmos. Meas. Tech.* 6(7): 1659-1671. doi:
1188 10.5194/amt-6-1659-2013.
1189 Targino, A. C., Coe, H., Cozic, J., Crosier, J., Crawford, I., Bower, K., Flynn, M., Gallagher, M.,
1190 Allan, J., Verheggen, B., Weingartner, E., Baltensperger, U. and Choularton, T. (2009).

1191 Influence of particle chemical composition on the phase of cold clouds at a high-alpine
1192 site in Switzerland. *J. Geophys. Res.* 114. doi: 10.1029/2008jd011365.
1193 Thevenon, F., Chiaradia, M., Adatte, T., Hueglin, C. and Pote, J. (2012). Characterization of
1194 Modern and Fossil Mineral Dust Transported to High Altitude in the Western Alps:
1195 Saharan Sources and Transport Patterns. *Adv. Meteorol.* doi: 10.1155/2012/674385.
1196 Van Dingenen, R., Raes, F., Putaud, J. P., Baltensperger, U., Charron, A., Facchini, M. C.,
1197 Decesari, S., Fuzzi, S., Gehrig, R., Hansson, H. C., Harrison, R. M., Huglin, C., Jones, A.
1198 M., Laj, P., Lorbeer, G., Maenhaut, W., Palmgren, F., Querol, X., Rodriguez, S.,
1199 Schneider, J., ten Brink, H., Tunved, P., Torseth, K., Wehner, B., Weingartner, E.,
1200 Wiedensohler, A. and Wahlin, P. (2004). A European aerosol phenomenology-1: physical
1201 characteristics of particulate matter at kerbside, urban, rural and background sites in
1202 Europe. *Atmos. Env.* 38(16): 2561-2577. doi: 10.1016/j.atmosenv.2004.01.040.
1203 Verheggen, B., Cozic, J., Weingartner, E., Bower, K., Mertes, S., Connolly, P., Gallagher, M.,
1204 Flynn, M., Choularton, T. and Baltensperger, U. (2007). Aerosol partitioning between the
1205 interstitial and the condensed phase in mixed-phase clouds. *J. Geophys. Res.* 112(D23).
1206 doi: 10.1029/2007jd008714.

1207 Weingartner, E., Nyeki, S. and Baltensperger, U. (1999). Seasonal and diurnal variation of
1208 aerosol size distributions (10 < D < 750 nm) at a high-alpine site (Jungfraujoch 3580 m
1209 asl). *J. Geophys. Res.* 104(D21): 26809-26820. doi: 10.1029/1999jd900170.
1210 Weingartner, E., Gysel, M. and Baltensperger, U. (2002). Hygroscopicity of aerosol particles at
1211 low temperatures. 1. New low-temperature H-TDMA instrument: Setup and first
1212 applications. *Env. Sci. Technol.* 36(1): 55-62. doi: 10.1021/es010054o.
1213 Weingartner, E., Saathoff, H., Schnaiter, M., Streit, N., Bitnar, B. and Baltensperger, U. (2003).
1214 Absorption of light by soot particles: determination of the absorption coefficient by means
1215 of aethalometers. *J. Aerosol Sci.* 34(10): 1445-1463. doi: 10.1016/s0021-8502(03)00359-
1216 8.
1217 WMO/GAW. (2003). *Aerosol Measurement Procedures Guidelines and Recommendations*.
1218 World Meteorological Organization, Geneva, Switzerland.
1219 Worringen, A., Kandler, K., Benker, N., Dirsch, T., Mertes, S., Schenk, L., Kästner, U., Frank,
1220 F., Nillius, B., Bundke, U., Rose, D., Curtius, J., Kupiszewski, P., Weingartner, E.,
1221 Vochezer, P., Schneider, J., Schmidt, S., Weinbruch, S., and Ebert, M. (2015). Single-
1222 particle characterization of ice-nucleating particles and ice particle residuals sampled by
1223 three different techniques. *Atmos. Chem. Phys.* 15: 4161-4178. doi:10.5194/acp-15-4161-
1224 2015.

Zellweger, C., Ammann, M., Buchmann, B., Hofer, P., Lugauer, M., Ruttimann, R., Streit, N., Weingartner, E. and Baltensperger, U. (2000). Summertime NO_y speciation at the Jungfraujoch, 3580 m above sea level, Switzerland. *J. Geophys. Res.* 105(D5): 6655-6667. doi: 10.1029/1999jd901126.

Zellweger, C., Forrer, J., Hofer, P., Nyeki, S., Schwarzenbach, B., Weingartner, E., Ammann, M. and Baltensperger, U. (2003). Partitioning of reactive nitrogen (NOy) and dependence on meteorological conditions in the lower free troposphere. *Atmos. Chem. Phys.* 3: 779-796.

Zieger, P., Fierz-Schmidhauser, R., Gysel, M., Ström, J., Henne, S., Yttri, K. E., Baltensperger, U. and Weingartner, E. (2010). Effects of relative humidity on aerosol light scattering in the Arctic. *Atmos. Chem. Phys.* 10(8): 3875-3890. doi:10.5194/acp-10-3875-2010.

Zieger, P., Kienast-Sjoegren, E., Starace, M., von Bismarck, J., Bukowiecki, N., Baltensperger, U., Wienhold, F. G., Peter, T., Ruhtz, T., Collaud Coen, M., Vuilleumier, L., Maier, O., Emili, E., Popp, C. and Weingartner, E. (2012). Spatial variation of aerosol optical properties around the high-alpine site Jungfraujoch (3580 m a.s.l.). *Atmos. Chem. Phys.* 12(15): 7231-7249. doi: 10.5194/acp-12-7231-2012.

Zieger, P., Fierz-Schmidhauser, R., Weingartner, E. and Baltensperger, U. (2013). Effects of relative humidity on aerosol light scattering: results from different European sites. *Atmos. Chem. Phys.* 13(21): 10609-10631. doi: 10.5194/acp-13-10609-2013.

1243

1244

1245 Table 1: List of continuously measured aerosol parameters and instruments at the Jungfraujoch (JFJ).
1246 Additional short-term measurements are mentioned and referenced in the text.

Parameter	**Employed method or instrument**	**Long-term measuring period**	**Technical description of instrument use at the JFJ[*2]**
Mass concentration:			
PM1	Betagauge (Eberline Inc.)	2.2004 – 6.2014	
TSP	Betagauge (Eberline Inc.)	6.2004 – 12.2006	
PM10	Betagauge (Eberline Inc.)	1.2007 – ongoing	
TSP	HiVol, Gravimetry (every 2nd day)	4.1973 – 12.2005	
PM10	HiVol, Gravimetry (daily)	1.2006 – ongoing	
Major chemical components in two size fractions [*1] (PM1 and TSP)	Inorganic fraction: Ion chromatography (sampling every 6th day)	7.1999 – ongoing	Henning *et al.* (2002), Cozic *et al.* (2008a)
Light absorption coefficients and equivalent black carbon at[*1]			Weingartner *et al.* (2003), Collaud Coen *et al.* (2010)
- a wavelength of 880 ± 50 nm	Aethalometer (AE10, Magee Inc.)	7.1995 – 3. 2001	
- 7 defined wavelengths	Aethalometer (AE31, Magee Inc.)	3.2001 – ongoing	
- 637 nm	MAAP (Carusso)	3.2003 – ongoing	
- 7 defined wavelengths	Aethalometer (AE33, Magee Inc.)	10.2014 – ongoing	
Light scattering and backscattering coefficient at 3 defined wavelengths[*1]	Nephelometer TSI 3563 (TSI Inc.) Aurora 3000 (Ecotech Inc.)	7.1995 – ongoing 11.2013 – ongoing	
Number concentration[*1]	Condensation Particle Counter		
N > 3 nm	CPC 3025 (TSI Inc.)	7.1995 – 3.1997	
N > 10 nm	CPC 3010 (TSI Inc.)	3.1997 – 3.2009	
N > 10 nm	CPC 3772 (TSI Inc.)	6.2008 - ongoing	
Aerosol size distribution[*1]			
$D_{mobility}$ = 18 – 750 nm	Scanning mobility particle sizer (SMPS)	1997/98	Weingartner *et al.* (1999)
$D_{mobility}$ = 20 – 600 nm	Scanning mobility particle sizer (SMPS)	1.2008 - ongoing	Jurányi *et al.* (2011)
$D_{optical}$ = 0.3 – 20 µm	Optical particle size spectrometer (Dust monitor 1.108, Grimm Inc.)	1.2008 - ongoing	Bukowiecki *et al.* (2011)
CCN number concentration [*1] (at various supersaturations)	Cloud condensation nuclei counter (CCNC, DMT Inc.)	4.2008 – ongoing	Jurányi *et al.* (2011)

1247 [*1] Measured at RH ~ 10% (fulfilling the recommendations by WMO/GAW, 2003) and laboratory temperature behind a heated inlet (see
1248 Weingartner *et al.*, 1999).

1249 [*2] Only technical references with a detailed discussion of JFJ specific instrument handling and data treatment are shown. Result-oriented
1250 references are discussed in the text.

1251

1252 Table 2: "The Jungfraujoch (JFJ) aerosol in a nutshell". Selected key parameters of the JFJ aerosol.

Parameter	**Value**					**References**
Aerosol relevant air mass characteristics						
FT conditions	Annual: 37%, summer: 20% (minimum), winter: 60% (maximum)					Herrmann *et al.* (2015) and references therein
Cloud presence	40% throughout the year					Baltensperger *et al.* (1998), Herrmann *et al.* (2015)
Number concentration						
$N_{> 10\ nm}$	cm^{-3}	Average	Median	0.25 perc.	0.75 perc	Condensation particle counter (TSI CPC 3010/3772, $N_{> 10\ nm}$) data 1997 – 2015, statistics from monthly averages (see Fig. 1 of this review)
	Annual	757	653	411	1000	
	Summer*	933	891	627	1176	
	Winter	563	416	274	675	
FT conditions	~35-50 cm^{-3} for accumulation mode particles ($N_{> 90\ nm}$)					Herrmann *et al.* (2015)
Nucleation events	up to 17'000 cm^{-3} ($N_{> 10\ nm}$)					
Size distribution						
Aitken mode	Modal diameter: 45 ± 11 nm (mean ± 1 standard deviation)					Herrmann *et al.* (2015)
Accumulation mode	Modal diameter: 135 ± 26 nm					
Chemical composition						
PM1	Organic matter (~51%), sulfate (~23%), ammonium (~14%), nitrate (~8%) and BC (~4%)					Fig. 2 of this review and references therein.
Coarse mode	Dominated by mineral dust (Saharan dust and rocks)					Section "Bulk chemical composition" of this review
Equivalent black carbon (EBC) (λ =880 nm)	ng m^{-3}	Average	Median	0.25 perc.	0.75 perc	Aethalometer (AE31) data 2001 – 2015, daily averages (see Fig. 1 of this review)
	Annual	55	33	15	73	
	Summer*	87	64	35	117	
	Winter	28	13	7	25	
Mass absorption cross section (MAC)	Winter: 7.6 $m^2\ g^{-1}$; summer 11 $m^2\ g^{-1}$(λ= 637 nm) Winter: ~10.2 $m^2\ g^{-1}$(λ = 637 nm)					Cozic *et al.* (2007) Liu *et al.*, (2010)
Optical properties						
Climatologies		Median	0.25 perc.	0.75 perc		
Scattering coefficient (λ =550 nm) [Mm^{-1}]	Annual	4.4	1.9	12.1		Andrews *et al.* (2011) and Fig. 4 of this review, data 1995-2007
	Summer*	8.2	3.1	26.9		
	Winter	1.5	0.3	2.9		
Absorption coefficient (λ =550 nm) [Mm^{-1}]	Annual	0.5	0.3	1.1		
	Summer*	0.9	0.4	2.0		
	Winter	0.3	0.2	0.5		
Single scattering albedo (λ =550 nm) [-]	Annual	0.92	0.88	0.94		
	Summer*	0.93	0.90	0.94		
	Winter	0.91	0.86	0.94		
Scattering Ångstrom coefficient [-]	Annual	1.59	0.68	2.28		
	Summer*	1.93	1.22	2.32		
	Winter	1.29	0.23	2.31		
Backscattered fraction (λ =550 nm) [-]	Annual	0.13	0.08	0.19		
	Summer*	0.13	0.10	0.16		
	Winter	0.14	0.05	0.22		
Saharan Dust Events (SDE)	Average without SDE		Average with SDE			Collaud Coen *et al.* (2004) and this review, data of 2001-2014.
Scattering coef. [Mm^{-1}] (λ =450 nm)	3.98		15.95			
Absorption coef. [Mm^{-1}] (λ =470 nm)	0.28		1.14			
N [cm^{-3}]	552		590			
SSA	0.92		0.92			
Scattering exponent $å_{sp}$	1.97		0.5			
Absorption exponent $å_{ap}$	1.1		1.48			
SSA exponent $å_{SSA}$	0.11		-0.07			

1253

1254 * increased PBL influence in summer

1255

1256 Table 2 (continued).

Parameter		**Value**									**References**
Optical properties (continued)											
Scattering enhancement *f*(RH) B: 450 nm; G: 550 nm; R: 700 nm		Average			Median			Standard deviation			Section "The effect of water uptake on the aerosol optical properties" of this review.
		B	G	R	B	G	R	B	G	R	
No SDE influence	γ	0.46	0.5	0.53	0.47	0.51	0.55	0.10	0.11	0.13	
	α	0.82	0.8	0.8	0.81	0.79	0.8	0.06	0.06	0.07	
	f(RH=85%)	1.96	2.06	2.19	1.99	2.09	2.24	0.07	0.07	0.09	
SDE events	γ	0.11	0.09	0.08	0.11	0.08	0.07	0.06	0.05	0.05	
	α	0.99	1.00	1.02	1.02	1.02	1.02	0.07	0.07	0.07	
	f(RH=85%)	1.24	1.19	1.17	1.24	1.19	1.16	0.08	0.08	0.08	
Aerosol hygroscopicity and CCN properties											
Mean growth factors at 90% RH		Average			Median		0.25 perc.		0.75 perc		Kammermann *et al.* (2010)
Dry particle diameter 50 nm	Annual	1.34			1.35		1.22		1.47		
	FT	1.36			1.37		1.24		1.49		
	SDE	1.35			1.36		1.19		1.51		
Dry particle diameter 110 nm	Annual	1.43			1.46		1.33		1.56		
	FT	1.45			1.48		1.35		1.58		
	SDE	1.44			1.48		1.32		1.58		
Dry particle diameter 265 nm	Annual	1.46			1.51		1.35		1.6		
	FT	1.47			1.52		1.37		1.61		
	SDE	1.42			1.48		1.2		1.6		
Hygroscopicity parameter κ	0.20 – 0.25 for particles larger than 80 nm										Kammermann *et al.* (2010), Jurányi *et al.* (2011), Fig. 6 of this review
CCN Climatology: CCN Number concentration N_{CCN}											
Supersaturation [%]	0.12	0.24	0.35	0.47	0.59	0.71	0.83	0.95	1.07	1.18	Jurányi *et al.* (2011)
Annual median	43	95	129	151	169	184	200	215	227	257	
Summer median*	99	205	280	330	366	411	447	473	471	527	
Winter median	17	40	51	61	68	74	82	88	94	114	
CCN Climatology: Activated Fraction $N_{CCN}/N_{>10nm}$											
Supersaturation [%]	0.12	0.24	0.35	0.47	0.59	0.71	0.83	0.95	1.07	1.18	Jurányi *et al.* (2011) and Fig. 7 of this review
Annual median	0.09	0.19	0.26	0.30	0.34	0.38	0.42	0.45	0.47	0.54	
Summer median*	0.12	0.27	0.37	0.42	0.48	0.53	0.58	0.61	0.63	0.70	
Winter median	0.03	0.07	0.10	0.12	0.14	0.16	0.18	0.19	0.20	0.26	
Aerosol-cloud interactions											
In-cloud aerosol characteristics		Average			Median		0.25 perc.		0.75 perc		Hammer *et al.* (2014a).
Peak supersaturation [%]: clouds arriving from NW					0.41		0.23		0.73		
Peak supersaturation [%]: clouds arriving from SE					0.22		0.14		0.45		
Peak supersaturation [%]: all clouds		0.45			0.35		0.21		0.61		
Activation threshold diameter [nm]: all clouds		98			87		65		113		
Ice nucleating particles and ice residual particles	<3 L^{-1} up to 40 L^{-1}										Section "Mixed-phase and glaciated clouds" of this review and references therein

1257

1258 * increased PBL influence in summer

1259

1260

List of Abbreviations

ACSM	Aerosol chemical speciation monitor
AMS	Aerosol mass spectrometer
AOD	Aerosol optical depth
BC	Black carbon
CCN/CCNC	Cloud condensation nuclei / Cloud condensation nuclei counter
CLACE	Cloud and aerosol characterization experiment
CO	Carbon monoxide
CPC	Condensation particle counter
EBC	Equivalent black carbon
EC	Elemental carbon
FT	Free troposphere
GAW	Global Atmosphere Watch
GF	Hygroscopic Growth Factor
HOA	Hydrocarbon-like organic aerosol
HTDMA	Hygroscopicity tandem differential mobility analyzer
JFJ	Jungfraujoch
INP	Ice nucleating particles

LWC	Liquid water content
MAC	Mass absorption cross section
NO_y	sum of oxidized nitrogen species
OC/OM	Organic carbon / organic matter
OOA	Oxygenated organic aerosol
OPSS	Optical particle size spectrometer
PBL	Planetary boundary layer
PM10, PM1	Mass concentration of particles with an aerodynamic diameter < 10 µm and < 1 µm, respectively
SDE	Saharan dust event
SMPS	Scanning mobility particle sizer
SSA	Single scattering albedo
TSP	Total suspended particles (mass concentration)
WINSOC	Water insoluble organic carbon
WMO	World Meteorological Organization
WSOC	Water soluble organic carbon

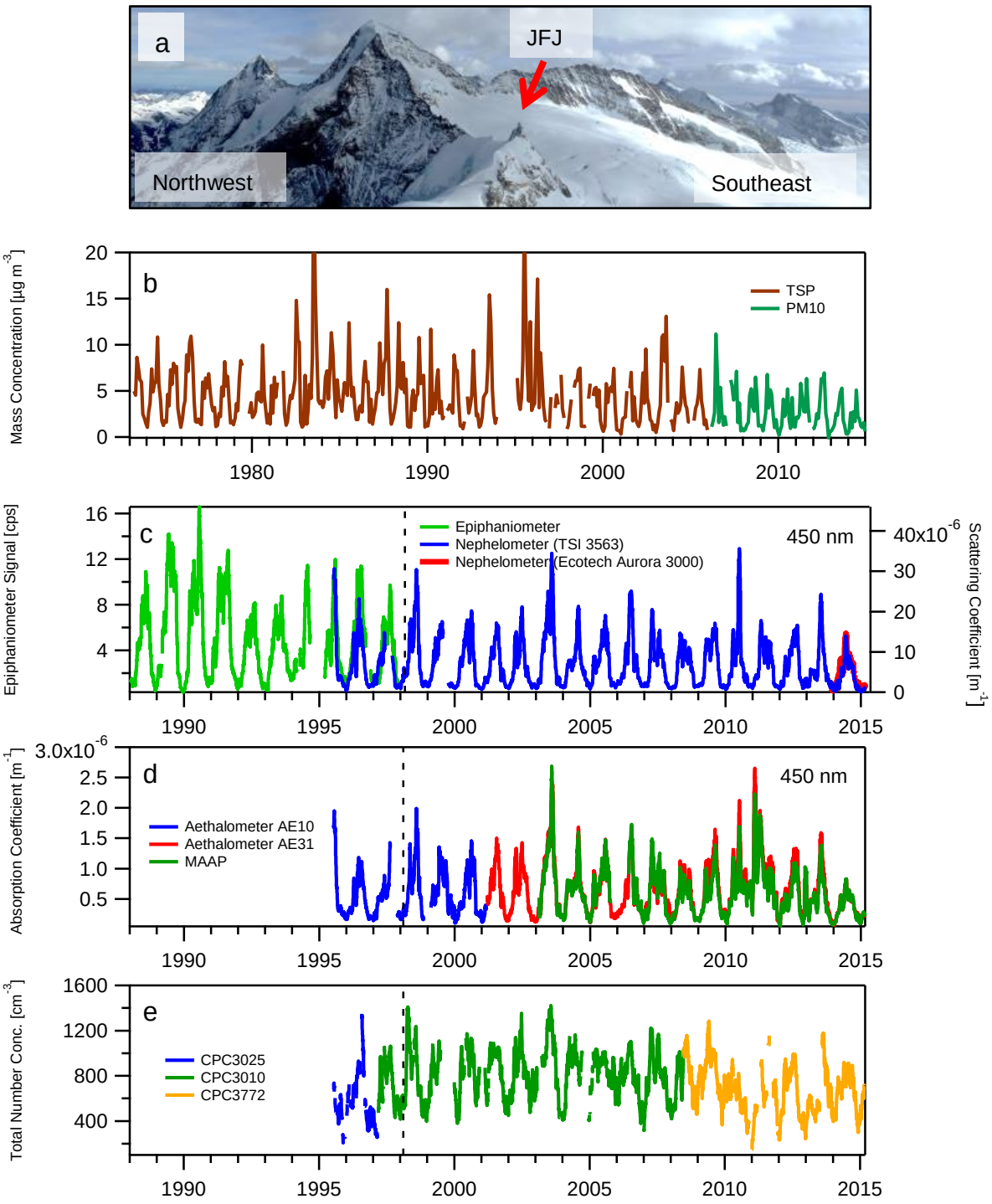

Fig. 1. Panel a: View of the station at Jungfraujoch (JFJ). Panels b-e: Temporal evolution of the continuously measured aerosol parameters at the Jungfraujoch. For TSP and PM10 monthly average values are shown, for the rest of the parameter the 30-day running average of the daily average values. The dashed vertical lines (Panels c-e) indicate that in January 1998, the entire aerosol laboratory was moved from the old JFJ research station (3454 m asl) to the JFJ Sphinx research station (3580 m asl) and a new inlet was employed (Weingartner *et al.*, 1999; Collaud Coen *et al.*, 2007). Gravimetric TSP and PM10 is sampled separately (see Table 1).

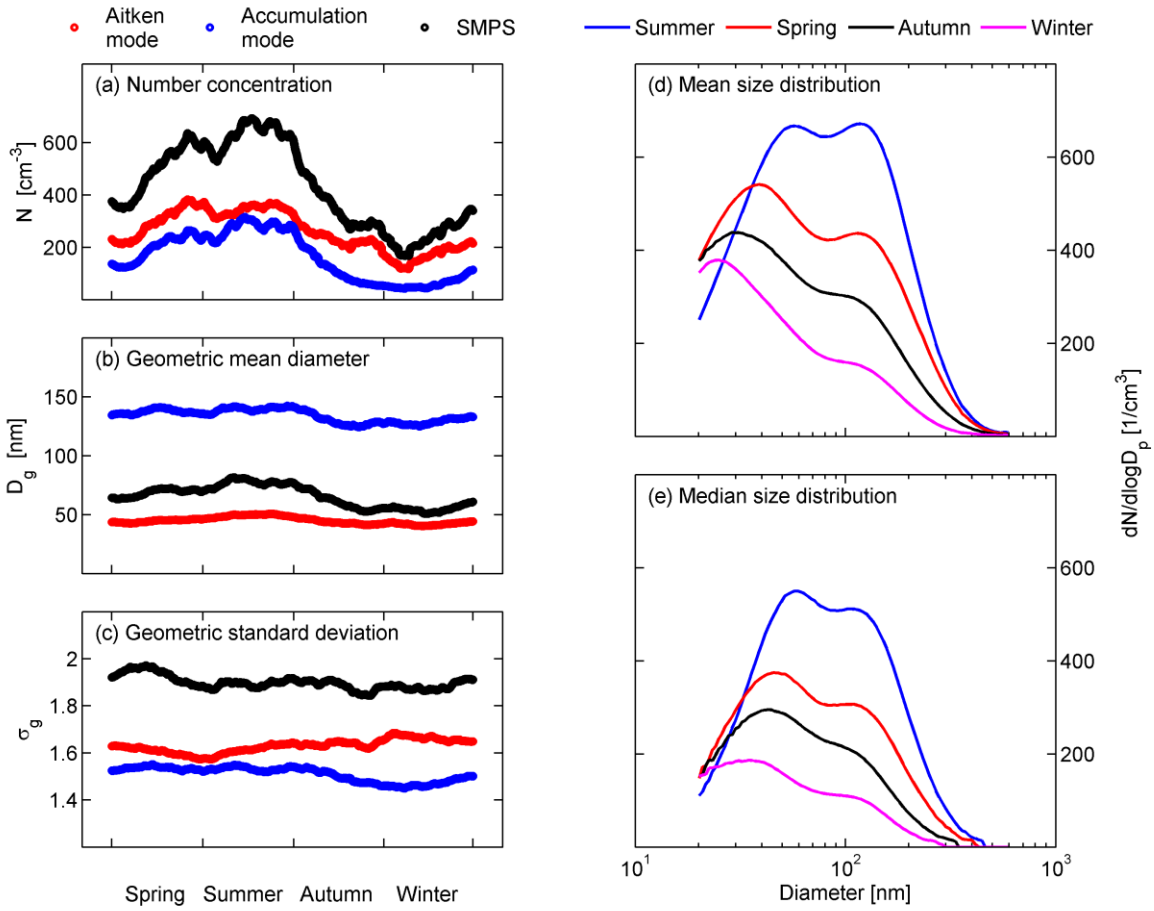

Fig. 2: Climatology and seasonal pattern of the aerosol number size distribution at the Jungfraujoch, adapted from Herrmann *et al.* (2015). The black lines in a), b) and c) show the integrated number concentration, the geometric mean diameter and the geometric standard deviation of the particle number size distribution, respectively (SMPS measurement between 20-600 nm). The red and blue lines in a), b), c) are the corresponding modal parameters of the Aitken and accumulation mode (obtained by multimodal lognormal fitting of 1h-average data followed by a 24h moving median and averaging of seasonal cycles over 6 years).

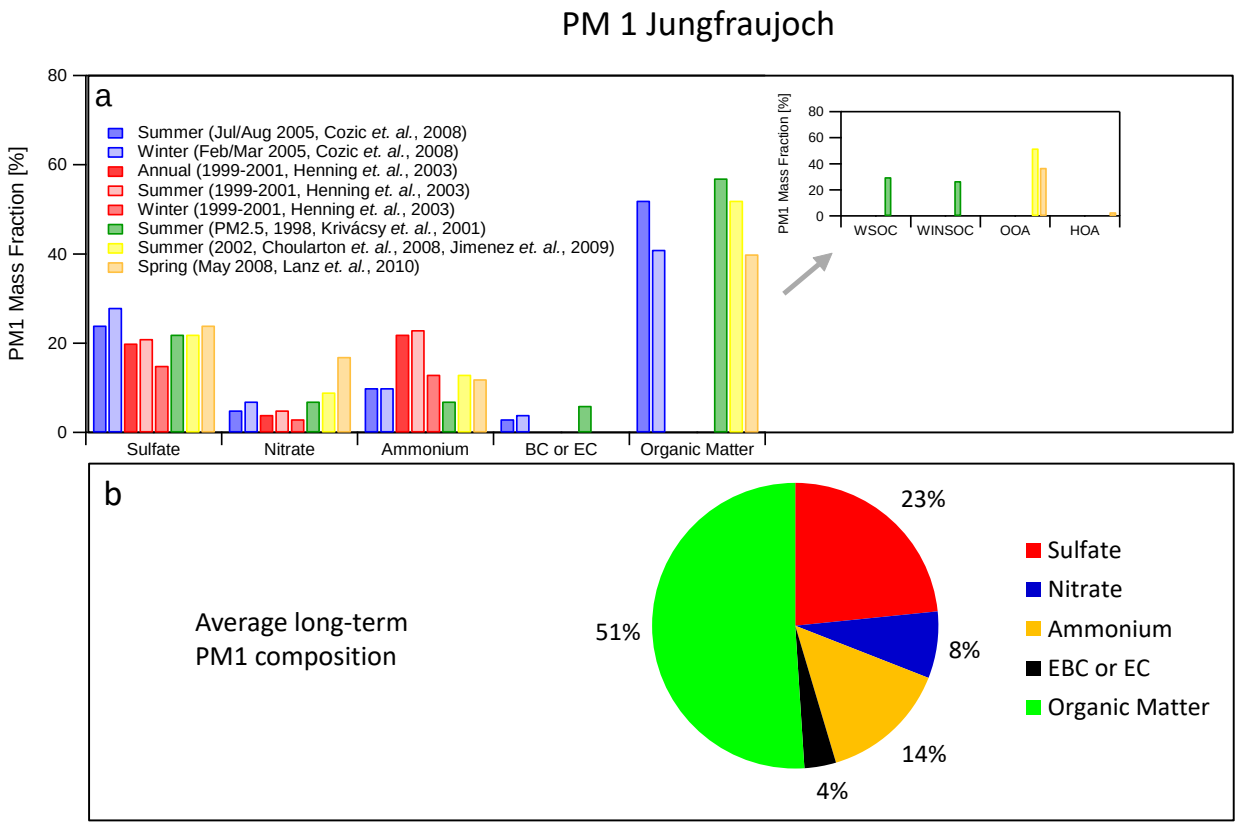

Fig. 3: PM1 bulk composition at the Jungfraujoch (JFJ). The upper panel lists available studies that present short-term, seasonal and/or annual chemical composition of PM1. For comparability, missing contributions to a full PM1 mass balance within the respective studies were estimated as follows. For the study by Henning *et al.* (2003) the long-term PM1/TSP mass ratio determined by Cozic *et al.* (2008a) was applied. The total non-refractory PM1 mass concentration presented in Choularton *et al.* (2008) /Jimenez *et al.* (2009) was upscaled by 5% to obtain total PM1, based on the study by Lanz *et al.* (2010). The lower panel shows the average composition based on the studies shown in the upper panel. EBC: Equivalent black carbon; EC: Elemental carbon; WSOC: Water soluble organic carbon; WINSOC: Water insoluble organic carbon; OOA: Oxygenated organic aerosol; HOA: Hydrocarbon-like organic aerosol.

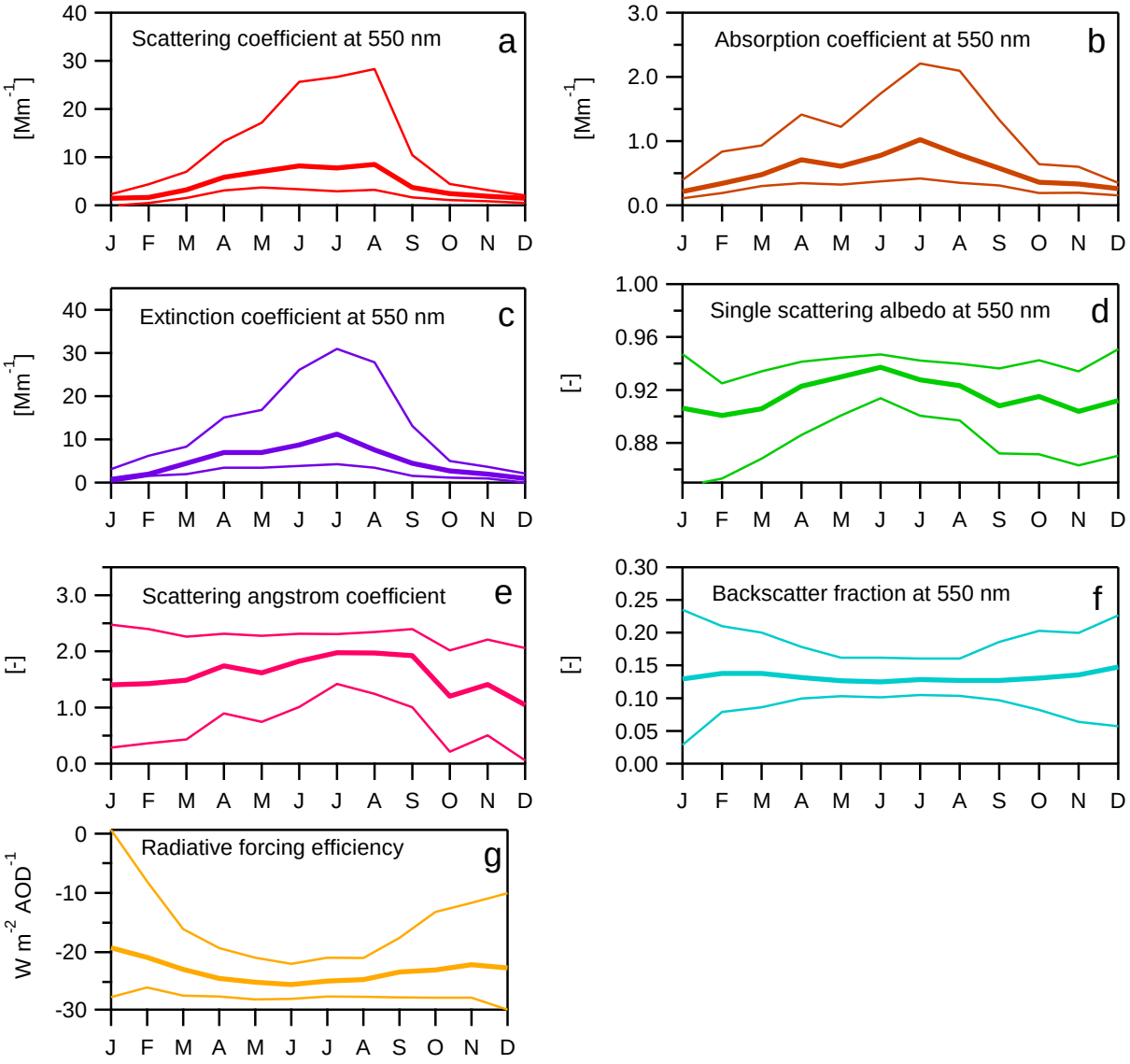

Fig. 4: Seasonal variation of dry optical aerosol properties at the Jungfraujoch from 1995 – 2007 (not corrected for scattering enhancement by water uptake), adapted from Andrews *et al.* (2011). The thick lines show the monthly median, and the thin lines the monthly 0.25 and 0.75 percentiles.

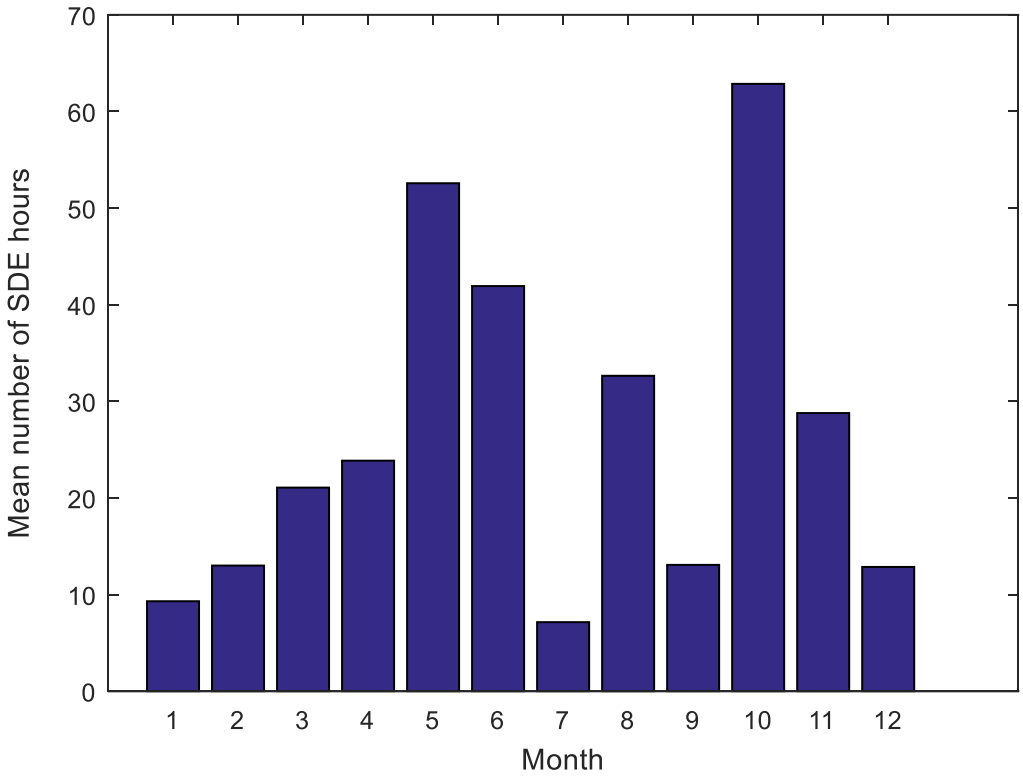

Fig. 5: Mean number of hours with SDE for the 2001-2014 period. In 2010 and 2011 construction activities at the JFJ impeded the SDE detection during most of these years.

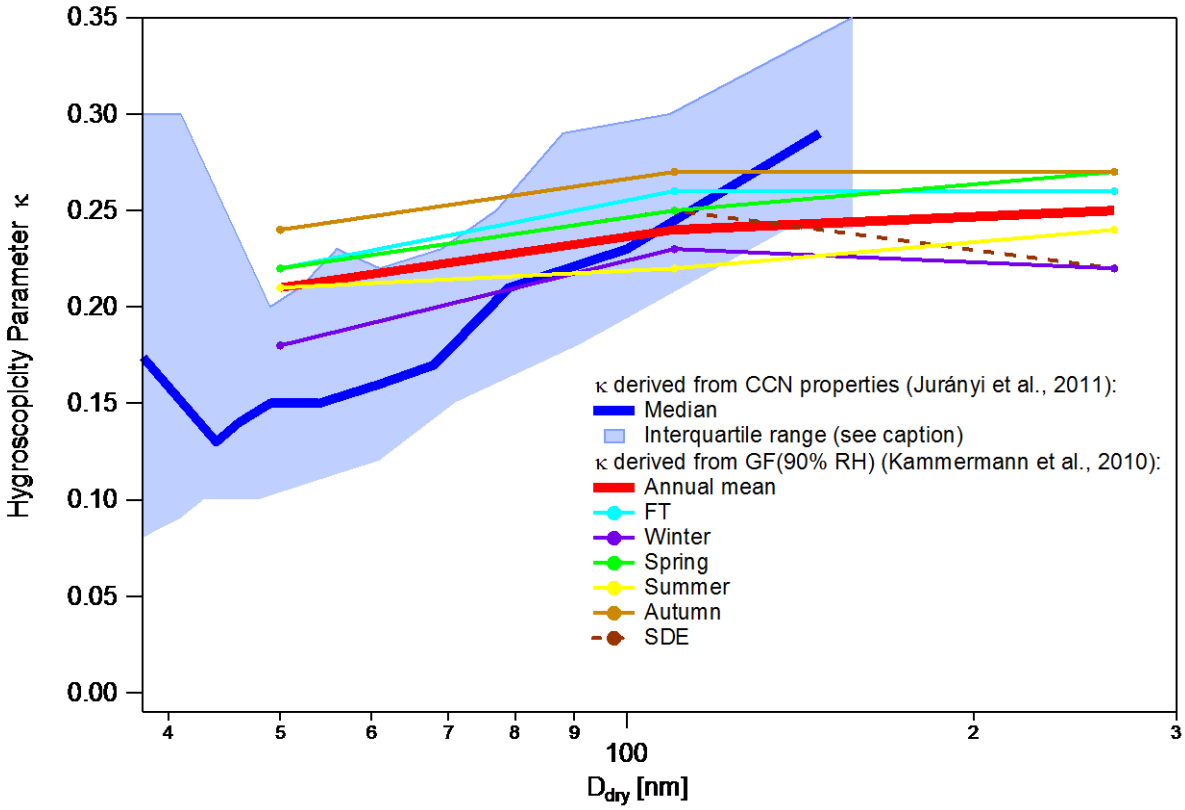

Fig. 6: Range of the hygroscopicity parameter κ found for the Jungfraujoch aerosol. κ derived from GF at RH=90% (Kammermann *et al.*, 2010) are shown as annual mean values as well as separated by seasons and air mass types. The median and interquartile range (25th to 75th percentage) are shown for CCN-derived κ from Juranyi *et al.* (2011).

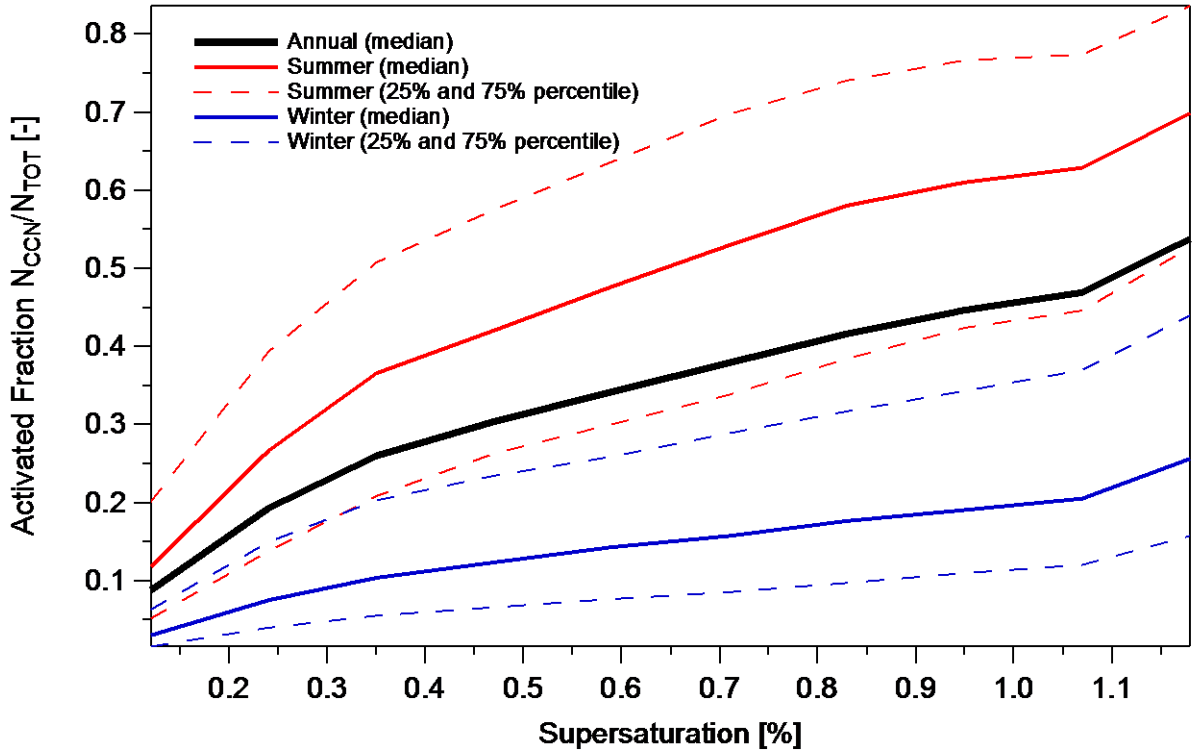

Fig. 7: CCN climatology at the Jungfraujoch. Activated fraction calculated with CCN number concentrations from Jurányi *et al.* (2011) divided by number concentration of particles with diameter <10 nm (N_{TOT}).

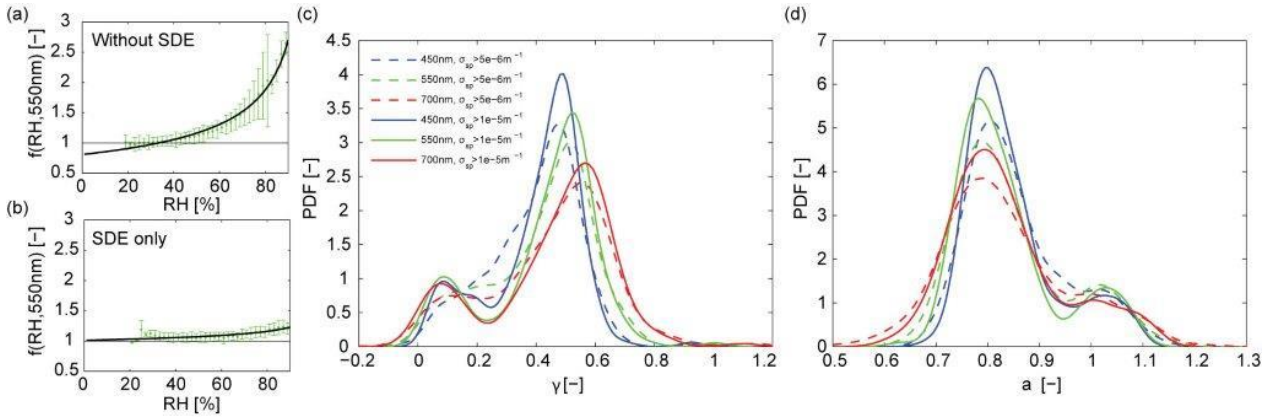

Fig. 8: The scattering enhancement factor *f*(RH) measured at JFJ during CLACE2010. (a) Average humidogram (at λ = 550 nm) for non-Saharan dust influenced periods. The error bars denote the standard deviation and the black line represents a fit using the *f*(RH)-parameterization of Eq. 2. (b) Same as panel (a) but for Saharan dust periods only. Panel (c) and (d) show the probability density functions of the *f*(RH)-fit parameters for the entire campaign for all nephelometer wavelengths and for two different thresholds of the particle scattering coefficient (see legend). The bimodal structure shows the two predominant cases for *f*(RH) at the JFJ: The background and PBL influenced aerosol (second local maxima in panel c, vice versa in panel d) and the Saharan dust episodes (first local maxima in panel c, vice versa in panel d).

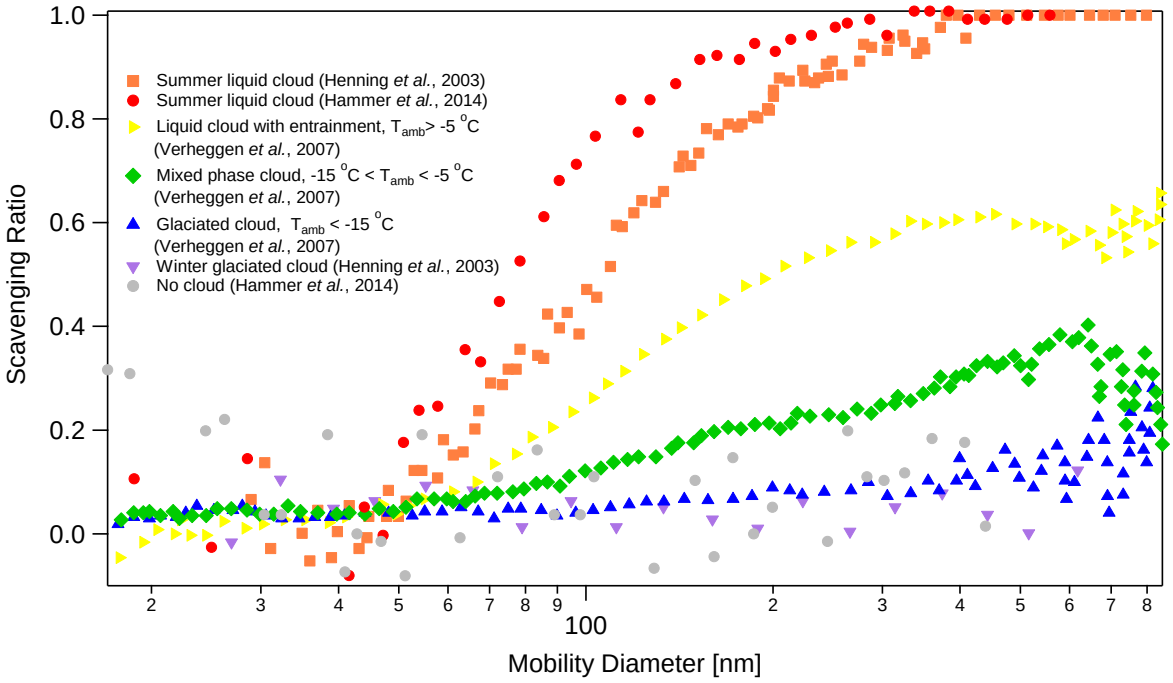

Fig. 9: Size resolved scavenging ratios found in liquid, mixed-phase and glaciated clouds at the JFJ.